Plasticity in striatal dopamine release is governed by release-independent depression and the dopamine transporter

Mark D. Condon[1], Nicola J. Platt[1], Yan-Feng Zhang[1], Bradley M. Roberts[1], Michael A. Clements[1], Stefania Vietti-Michelina[1], Min-Yee Tseu[1], Katherine R. Brimblecombe[1], Sarah Threlfell[1,2], Ed O. Mann[1] and Stephanie J. Cragg[1,2]*

[1]Department of Physiology, Anatomy and Genetics, Parks Road, University of Oxford, OX1 3PT, UK

[2]Oxford Parkinson's Disease Centre, Oxford, OX1 3PT

*Author for Correspondence: Stephanie.cragg@dpag.ox.ac.uk, +44 1865 282513

Short Title: Short-term plasticity in dopamine release

Keywords: Dopamine, striatum, release probability, dopamine release, short-term plasticity, short-term depression, short-term facilitation, dopamine transporter, release-independent depression, axonal excitability, voltammetry

Key Findings:

- Short-term plasticity in dopamine release is only weakly governed by initial release
- Short-term depression is strongly dependent on axonal excitability and activation
- The dopamine transporter controls short-term plasticity and drives short-term depression
- Dopamine transporters govern the balance between release-dependent and -independent mechanisms

Abstract

Mesostriatal DA neurons possess extensively branched axonal arbours. Whether action potentials are converted to DA output in striatum will be influenced dynamically and critically by axonal properties and mechanisms that are poorly understood. We addressed the roles for mechanisms governing release probability and axonal activity in determining short-term plasticity of DA release, using fast-scan cyclic voltammetry in *ex vivo* mouse striatum. Brief short-term facilitation (STF) and longer short-term depression (STD) were only weakly dependent on the level of initial release, i.e. were release-insensitive. Rather, short-term plasticity was strongly determined by mechanisms which governed axonal activation, including K^+-gated excitability and the dopamine transporter (DAT), particularly in dorsal striatum. We identify the DAT as a master regulator of DA short-term plasticity, governing the balance between release-dependent and independent mechanisms that also show region-specific gating.

Introduction

Dopamine (DA) release in the striatum plays key roles in action selection and behavioural reinforcement, and is dysregulated in diverse disorders including Parkinson's disease and addictions. DA neurons generate action potentials at a range of frequencies, firing tonically below 10 Hz, and intermittently in short bursts with instantaneous frequencies of up to approximately 40 Hz [1-6]. Bursts occur in response to salient environmental stimuli predicting reward value or action signals [6-8]. However, the extent to which action potential activity is conveyed into striatal DA release remains unclear; DA axons are important sites for local regulation of DA output [9-13] which shows strong short-term plasticity and distorts the relationship between activity and DA output [11,14-17].

Despite classical accounts of axons as simple high-fidelity cables, neurotransmitter release following action potentials in CNS neurons is shaped by factors that regulate action potential propagation and axonal excitability such as axonal morphology and branching, the expression of ion channels and presynaptic receptors, and other diverse mechanisms that regulate vesicle pools, neurotransmitter release probability

43 and short-term plasticity [18]. Axons of DA neurons are remarkable: they comprise vast, extensively
44 branched arbours [19,20], that from anatomical observations and a binary tree model [21] can be calculated
45 to form an average of 16,000 branch points per nigrostriatal neuron. Axonal properties are likely to be
46 particularly important in governing axonal activity and striatal DA output. One major influence is the input
47 from striatal cholinergic interneurons onto nicotinic receptors (nAChRs) on DA axons, which influence the
48 pattern of DA release and promote short-term depression (STD) [11,15,22-24]. But even in the absence of
49 nAChR activation, DA release shows an underlying spectrum of short-term plasticity ranging from short-term
50 depression (STD) to short-term facilitation (STF) [11,15,23,25,26] for which the underlying mechanisms are
51 poorly understood. Existing evidence suggests that short-term plasticity might be only weakly related to
52 initial levels of release [17,25,26] but the dominant drivers remain undefined.

53 Here, we delineate the roles of three types of intrinsic drivers that could underlie short-term
54 plasticity of DA release from striatal DA axons. We examine, firstly, the role for initial release; secondly, the
55 role for K^+-dependent mechanisms that will govern overall excitability and repolarization; and thirdly, a
56 potential role for the dopamine transporter (DAT). Besides mediating DA uptake, the DAT generates a
57 depolarising transport-coupled conductance in midbrain DA neurons [27,28], and has been suggested to
58 limit vesicular release [29-32]. Thus, the DAT has the potential to govern short-term plasticity of DA release
59 via regulation of axonal activation and/or release probability (P_r).

60 We reveal that initial release plays a limited role in short-term plasticity except on the shortest of
61 timescales (10 - 25 ms), when STF operates. The prevailing STD at longer timescales (25 ms – 200 ms) is
62 apparently independent of the level of initial release i.e. it is “release-insensitive”. We identify that STD is
63 strongly determined by mechanisms that influence membrane activation, particularly in dorsal striatum.
64 Furthermore, we identify that the DAT drives STF at shortest intervals and STD at longer, physiological inter-
65 pulse intervals, effectively clamping release. We propose a region-specific hierarchy of interacting drivers of
66 short-term plasticity, overseen by the DAT, with the DAT promoting release-insensitive over release-
67 dependent mechanisms.

68 # Results

69 ## Patterns of short-term plasticity at DA release sites are region-specific and weakly release-
70 dependent

71 We assessed short-term plasticity of DA release in acute coronal striatal slices evoked using pairs of local
72 electrical pulses and inter-pulse intervals (IPI) of 10-200 ms in both dorsolateral striatum (caudate-putamen,
73 CPu) and nucleus accumbens core (NAc). Confounding effects of nAChRs were excluded by inclusion
74 throughout of antagonist DHβE (see Methods). The ratio of DA release evoked by the second pulse in a pair
75 compared to a single pulse (paired-pulse ratio, PPR) varied with IPI in CPu (**Fig. 1A,C**) and in NAc (**Fig. 1B,C**).
76 In both regions, PPR decreased with increasing IPI. Short-term facilitation (STF, PPR>1) was observed at the
77 shortest IPIs (10 ms in CPu, 10-25 ms in NAc), whereas strong short-term depression (STD) (PPR<1) was
78 observed at longer IPIs in both regions (≥ 25 ms in CPu, >40 ms in NAc), as shown previously [15,33]. In CPu,
79 STD was significantly more pronounced than in NAc (**Fig. 1C,** Two-way ANOVA, region x IPI interaction, $F_{4,25}$ =
80 4.195, P = 0.010, n = 7) suggesting region-specific gating of short-term plasticity.

81 PPR at classic fast synapses is typically inversely related to initial P_r, resulting in STF when P_r is low,
82 and STD when P_r is high [34-37]. STF at these synapses consists of several temporally-overlapping processes
83 with a range of time constants from 30 – 500 ms [38]. An inverse relationship between PPR and single pulse
84 release has been reported in CPu for short IPI of 10 ms but not 100 ms [25], suggesting that short-term
85 plasticity of DA release might reflect initial P_r at only very short intervals. We probed the relationship
86 between PPR and the extracellular concentration of DA ($[DA]_o$) evoked by a single pulse (as a proxy of initial
87 P_r) in CPu and in NAc across a population of release sites that exhibited a 10-fold range in $[DA]_o$ evoked by a
88 single pulse (1p $[DA]_o$). We found an inverse relationship between 1p $[DA]_o$ and PPR for IPI of 10 ms in both
89 CPu and NAc, and at 40 ms in NAc only, but in neither region at the longer interval of 100 ms (**Fig. 1D,** linear
90 regressions, 10 ms, CPu: β = -0.79 ± 0.14 [95% CI: -1.08 to -0.50], $F_{1,33}$ = 30.9, P = 3.56 x 10^{-6}, n = 35; NAc: β = -
91 0.52 ± 0.19 [95% CI: -0.93 to -0.11], $F_{1,17}$ = 7.136, P = 0.016, n = 19; 40 ms, CPu, P = 0.152, n = 35; NAc 95% CI:

92 -0.38 to -0.001], $F_{1, 17}$ = 4.489, *P* = 0.049, *n* = 19; 100 ms, CPu: *P* = 0.122, n = 35; NAc: *P* = 0.917, n = 19). These
93 data indicate that DA PPR is a function of P_r at only very short intervals and specifically, only at those
94 intervals at which STF can be observed. These data suggest that short-term plasticity in DA release might be
95 governed by release-dependent mechanisms at very short intervals, but by mechanisms unrelated to initial
96 release at longer more physiological intervals.

97 This expression of STD was not due to activation of inhibitory D_2-autoreceptors (D2Rs). Antagonism
98 of D2Rs with antagonist L741,626 (1 µM), did not influence peak $[DA]_o$ (**Fig. 1E**) or PPR at IPIs up to 200 ms in
99 either CPu or NAc (**Fig. 1F**, Two-way ANOVA, CPu: *P* = 0.420, n= 5, NAc: *P* = 0.2197, n = 6), although did for
100 longer IPIs (**Supp. Fig S1**) consistent with previous findings that D2Rs only modify release after longer IPIs
101 (>200 ms, < 3 s) and are not tonically regulating DA release in brain slices [14,39-41]. We also ruled out an
102 alternative effect whereby DA remaining after the first pulse might determine the release by the second,
103 with higher DA remaining at short IPI driving STF and lower DA at longer IPI driving STD. We varied the
104 intensity of the initial electrical stimulus to halve the $[DA]_o$ evoked in CPu, but showed that the $[DA]_o$ evoked
105 by a second pulse at a fixed IPI of 25 ms and a fixed stimulus strength released the same $[DA]_o$ at P2
106 regardless of initial level of $[DA]_o$ (**Suppl. Fig S2**).

107 Short-term plasticity is shaped by calcium-dependent facilitation and release-insensitive
108 depression

109 To test directly whether short-term plasticity can be shaped by changes to P_r, we varied initial release at a
110 given release site by varying the extracellular concentration of Ca^{2+} ($[Ca^{2+}]_o$) in a 3-fold range (1.2 - 3.6 mM).
111 $[DA]_o$ evoked by 1p was strongly dependent on $[Ca^{2+}]_o$, in both CPu and NAc (**Fig. 2A,B**) as expected. There
112 was a steeper relationship between $[Ca^{2+}]_o$ and 1p $[DA]_o$ in CPu than in NAc (**Fig. 2C**, Two-way ANOVA, $[Ca^{2+}]_o$
113 x region interaction, $F_{2,20}$ = 17.25, *P* = 4.43 x10^{-5}, *n* = 6), consistent with previous findings [26]. However,
114 despite large changes in 1p-evoked DA release in both regions (4-fold in CPu, 2.5-fold in NAc), $[Ca^{2+}]_o$ had
115 only modest effects on PPR limited to very short intervals. In CPu, a trend towards an inverse relationship at
116 10 ms IPI did not reach significance (**Fig. 2D,F**, Two-way ANOVA, *P* = 0.604, n = 4). In NAc, PPR varied

117 inversely with $[Ca^{2+}]_o$ but at only the shortest interval of 10 ms IPI (**Fig. 2E,F,** Two-way ANOVA, IPI x $[Ca^{2+}]_o$
118 interaction, $F_{8,30} = 4.497$, $P = 0.001$, $n = 3$). Furthermore, we noted that the size of effect on PPR in NAc
119 versus CPu did not tally with the size of effect of $[Ca^{2+}]_o$ on 1p $[DA]_o$: the range of 1p $[DA]_o$ were less in NAc
120 than CPu despite the larger range in short-term plasticity (**Fig. 2F**). The difference in short-term plasticity
121 between CPu and NAc cannot therefore be attributed to a difference in the sensitivity of initial P_r to $[Ca^{2+}]_o$
122 (see Fig. 2C). Together these data show that short-term plasticity of DA release is not easily explained by
123 Ca^{2+}-limited mechanisms, suggesting that other mechanisms dominate that are independent of initial
124 release.

125 To confirm that STD and its insensitivity to $[Ca^{2+}]$ do not result from stimulation of an undefined
126 input to DA axons, we used targeted optogenetic stimulation of DA axons. In striatum from heterozygote
127 $DAT^{IRES\text{-}Cre}$ mice expressing ChR2-eYFP after viral delivery, a brief light flash (2 ms, 473 nm wavelength)
128 evoked $[DA]_o$ transients that varied with $[Ca^{2+}]_o$ (**Fig. 2G**) and with a steeper $[Ca^{2+}]_o$ concentration-response
129 curve in CPu than in NAc (**Fig. 2H**, nonlinear regression, CPu: $R^2 = 0.91$, n = 3, NAc: $R^2 = 0.94$, n = 3,
130 comparison of fits: $F_{4,118} = 5.94$, $P = 2 \times 10^{-4}$), as seen for electrically evoked DA release. Furthermore, at an
131 interval of 40 ms, at which ChR2 can reliably drive repeat spiking in DA neurons [1] and DA release [11], PPR
132 was greater in NAc than in CPu, as observed using electrical stimulation (see Fig. 1C). However, even with
133 optogenetic stimulation, there was no inverse relationship between PPR and 1p $[DA]_o$ (**Fig. 2I,** linear
134 regression, CPu: $P = 0.874$, n = 3, NAc: $P = 0.286$, n = 3). These data confirm that STD is not attributable to
135 stimulation of other inputs. For subsequent experiments, we chose electrical over optogenetic stimulation to
136 avoid the potentially confounding effects of Ca^{2+} entry through ChR2 on P_r and short-term plasticity.

137 Release-independent STD is controlled by K^+-dependent gating

138 We tested whether STD was gated by axonal membrane excitability by varying $[K^+]_o$. Varying $[K^+]_o$ can alter
139 membrane potential and repolarisation through the Nernstian driving forces underlying K^+-mediated
140 currents [42] and also through K^+-dependent inhibition of K^+-channel inactivation [43]. Reduced $[K^+]_o$ can
141 thereby favour membrane hyperpolarisation and faster repolarisation between pulses, promoting de-

142 inactivation of Na^+ channels, but can also promote inactivation of K^+-channels, leading to use-dependent
143 depolarisation and enhanced Na^+-channel recruitment. In either case, recruitment of voltage-gated Na^+
144 channels at a subsequent depolarising event will be altered.

145 We found that varying $[K^+]_o$ (1.25 - 7.5 mM) did not change 1p $[DA]_o$ in either CPu (**Fig. 3A**) or NAc
146 (**Fig. 3B**) but nonetheless significantly modulated short-term plasticity (**Fig. 3A-D**). In CPu, PPR varied
147 inversely with $[K^+]_o$ across IPIs, with STD minimized at lowest $[K^+]_o$ (**Fig. 3C**, Two-way ANOVA, $[K^+]_o$ x IPI
148 interaction, $F_{8,30} = 7.66$, $P = 1.53 \times 10^{-5}$, $n = 3$). In NAc, the effect of $[K^+]_o$ on PPR was less evident than in CPu,
149 but showed an overall significance (**Fig. 3D**, Two-way ANOVA, main effect of $[K^+]_o$, $F_{2,30} = 15.15$, $P = 2.83 \times 10^{-}$
150 ^{5}, $n = 3$). Since we observed no effect of $[K^+]_o$ on 1p $[DA]_o$, these effects on PPR were unrelated to initial P_r at
151 either short (10 ms) or longer (100 ms) IPI (**Fig. 3E,** vertical slopes). These findings demonstrate directly that
152 short-term plasticity of DA release can be dissociated from initial release, i.e. there is a release-insensitive
153 short-term plasticity. Furthermore, they suggest that STD is governed by mechanisms governing axonal
154 membrane polarisation/activation particularly in CPu.

155 To identify whether the control of short-term plasticity by $[K^+]_o$ is accounted for by voltage-
156 dependent effects, we tested whether the effects of $[K^+]_o$ on PPR could be substituted for, and prevented by
157 broadly blocking K_v channels. We hypothesised that a K_v blocker (4-aminopyridine, 4-AP) should promote
158 STD and prevent effects of changes in $[K^+]_o$. In CPu, broad inhibition of K_v channels by 4-AP (100 µM), unlike
159 changes in $[K^+]_o$ alone, profoundly increased 1p $[DA]_o$ (**Fig. 4A, B**, Two-way ANOVA, main effect of 4-AP: $F_{1,3}$ =
160 33.63, $P = 0.010$, $n = 4$). This effect is consistent with the expected widening of the action potential by 4-AP
161 [44] which will increase Ca^{2+} entry and neurotransmitter release for a single stimulus. In addition, 4-AP,
162 similar to the effects of high $[K^+]_o$ (see Fig. 3), but unlike high $[Ca^{2+}]_o$ (see Fig. 2), reduced PPR at all IPIs, and
163 also prevented the effects of changing $[K^+]_o$ on PPR (**Fig. 4C, 4D,** Two-way ANOVA, 4-AP x $[K^+]_o$ interaction, $F_{1,}$
164 $_{12} = 6.003$, $P = 0.031$, $n = 4$). These findings indicate that inhibition of K_v channels promotes STD, and suggest
165 that enhanced K_v currents relieve STD, and that hyperpolarizing/repolarizing conditions limit STD and
166 promote subsequent release.

167 In NAc, we observed no significant effect of 4-AP on 1p $[DA]_o$ (**Fig. 4E,F**, Two-way ANOVA, *P* = 0.266,
168 n = 3). However, 4-AP did decrease PPR at all IPIs, and there was no effect of varying $[K^+]_o$ in control
169 conditions or in the presence of 4-AP (**Fig. 4G, H**). These findings verify that STD can be distinct from the
170 effects on initial P_r and identify that STD is underpinned by the gating of axonal excitability.

171 K^+-dependent gating does not alter release-dependence of short-term plasticity

172 We investigated whether $[K^+]_o$-dependent STD could be a limiting factor that prevents short-term plasticity
173 of DA release from responding to changes in P_r or whether yet further regulatory mechanisms might be
174 indicated. We relieved STD (using low $[K^+]_o$) to test whether we could unmask a sensitivity of short-term
175 plasticity to changes in initial release (using variation in $[Ca^{2+}]_o$). In CPu, 1p $[DA]_o$ varied with $[Ca^{2+}]_o$ in a
176 similar manner in 1 mM $[K^+]_o$ versus 5 mM $[K^+]_o$ (**Fig. 5A-C**) and although PPRs were elevated when $[K^+]_o$ was
177 low (**Fig. 5D**) (as seen in Figs. 3C, 4C), there was no significant interaction between $[K^+]_o$ and $[Ca^{2+}]_o$ at IPIs of
178 either 10 ms or 100 ms (**Fig. 5D**, Two-way ANOVA, 10 ms IPI: *P* = 0.086, 100 ms IPI: *P* = 0.654, n = 10). In NAc
179 also, 1p $[DA]_o$ varied with $[Ca^{2+}]_o$ in a manner that did not depend on $[K^+]_o$ (**Fig. 5E-G**) and there was no
180 significant interaction between the effects of $[K^+]_o$ and $[Ca^{2+}]_o$ on PPR at either 10 ms or 100 ms IPI (**Fig. 5H**,
181 Two-way ANOVA, 10 ms IPI: *P* = 0.963, 100 ms IPI: *P* = 0.883, n = 7). By limiting STD, we did not enhance Ca^{2+}-
182 dependent modulation of STF or STD in either CPu or NAc. Therefore, the mechanism through which $[K^+]_o$
183 modulates short-term plasticity is not masking or preventing short-term plasticity from being Ca^{2+}-limited, in
184 either CPu or NAc. This observation suggests that an additional mechanism may operate to limit the Ca^{2+}-
185 and release-dependence of short-term plasticity besides K_v-regulation of axonal excitability and polarization.

186 The dopamine transporter regulates short-term plasticity of dopamine release

187 Alongside its control of DA uptake, the dopamine transporter (DAT) has previously been shown to govern
188 underlying DA release processes [29-32]. The DAT is also known to mediate electrogenic currents during DA
189 binding and transport [27,45] that have been shown to modulate the membrane potential of DA neurons *in*

190 *vitro* [28]. We therefore investigated the hypothesis that DAT in striatum could consequently contribute to
191 short-term plasticity.

192 To avoid adaptations to release seen after DAT knockout, we used uptake inhibitors to inhibit DAT
193 function. We found that the monoamine uptake inhibitors cocaine and methylphenidate (MPH) and DAT
194 inhibitor nomifensine significantly altered the pattern of short-term plasticity in a common manner. Cocaine
195 (5 µM), MPH (5 µM) or nomifensine (10 µM) increased the peak amplitude and decreased the rate of decay
196 of $[DA]_o$ transients in CPu and NAc in keeping with DA uptake inhibition (**Fig. 6A,C,G,I**) and also prevented
197 STF and significantly relieved STD (Cocaine: **Fig. 6A,B**, Two-way ANOVA, cocaine x IPI interaction, $F_{4, 30}$ =
198 11.97, $P = 6.24 \times 10^{-6}$, $n = 4$, MPH: **Fig. 6C,D**, Two-way ANOVA, MPH x IPI interaction, $F_{4, 40} = 5.316$, $P = 0.002$,
199 $n = 5$; Nomifensine: **Fig. 6E,F**, Two-way ANOVA, nomifensine x IPI interaction, $F_{4, 80} = 21.12$, $P = 6.5 \times 10^{-12}$, n =
200 3). These findings indicate that the DAT is a key regulator of short-term plasticity of DA release. At shortest
201 IPI, DAT promotes STF, whereas at longer IPI, DAT clamps release to promote STD in CPu. In NAc, cocaine
202 and MPH (we did not test nomifensine) prevented STF at 10 ms IPI (**Fig. 6G,H,** Two-way ANOVA, cocaine x IPI
203 interaction, $F_{4, 30} = 7.884$, $P = 1.82 \times 10^{-4}$, $n = 4$; MPH: **Fig 6I,J,** Two-way ANOVA, MPH x IPI interaction, $F_{4, 20}$ =
204 3.986, $P = 0.016$, $n = 3$) but in contrast to CPu, STD at longer intervals was not relieved. In NAc, the DAT
205 regulated short-term plasticity at only short interpulse intervals. Since it is at these intervals that short-term
206 plasticity is related to P_r (see Fig 1), these data suggest that it is the effect of DAT inhibition on promoting
207 subsequent DA release that underlies its effects on short-term plasticity at short intervals in NAc.

208 We ruled out activation of D_2 receptors as contributing to DAT-mediated changes in short-term
209 plasticity. At longer interpulse intervals of 2-3 seconds when sufficient time has elapsed for D2 receptors to
210 have been activated, the D2 antagonist L-741626 in the presence of cocaine can enhance evoked $[DA]_o$ at a
211 second stimulus (**Suppl Fig. S3A,B**, Two-way ANOVA, main effect of L-741-626, $F_{1,64} = 28.96$, $P < 0.0001$, n =
212 4). However, the effect of cocaine on STF and STD at shorter intervals spanning 10-200 ms was not modified
213 by the D2 antagonist (**Suppl. Fig S3C**, Two-way ANOVA, main effect of L-741,626, $F_{1,20} = 2.76$, $P > 0.05$, n = 4).
214 We also ruled out potential local anaesthetic actions of cocaine on voltage-gated Na^+ channels (VGSCs), since

215 lidocaine (5 µM), an inhibitor of VGSCs, did not significantly alter short-term plasticity (**Supp Fig. S4**),
216 consistent with reports that cocaine does not inhibit VGSCs at the concentration used in this study [46].

217 We tested whether the effects of DAT inhibition on short-term plasticity were dependent on
218 synapsin III which has been suggested to mediate the role of the DAT in vesicle segregation and in limiting
219 release [29]. However, the effects of cocaine on short-term plasticity persisted in mice lacking synapsin III
220 (**Suppl. Fig. S5**), indicating that the DAT regulates short-term plasticity via a synapsin III-independent or other
221 redundant mechanism.

222 The DAT limits release-dependence of short-term plasticity in CPu

223 Since the DAT operates a clamp on DA release in CPu that drives STD, we tested whether the DAT might
224 prevent short-term plasticity from being Ca^{2+}- and release-dependent. We tested whether there was a
225 stronger relationship between $[Ca^{2+}]_o$ and PPR in CPu, in the presence of cocaine. There was no effect on PPR
226 of changing $[Ca^{2+}]_o$ in the absence of cocaine (**Fig. 7A,B**, Two-way ANOVA, $P = 0.209$, n = 4), but by contrast in
227 the presence of cocaine there was a significant effect of $[Ca^{2+}]_o$: PPR at IPIs of 10-40 ms were significantly
228 elevated in 1.2 versus 2.4 mM $[Ca^{2+}]_o$ (**Fig. 7A,C-E**, Two-way ANOVA, $[Ca^{2+}]_o$ x IPI interaction, $F_{3, 24} = 6.137$, $P =$
229 0.003, $n = 4$). There was a significantly stronger effect of $[Ca^{2+}]_o$ on PPR in the presence of cocaine than in
230 control conditions at 25 ms (**Fig. 7D;** Two-way ANOVA, cocaine x $[Ca^{2+}]_o$ interaction; $F_{1, 12} = 7.86$; $P = 0.016$; n
231 $= 4$) and 40 ms IPI (**Fig. 7D**; Two-way ANOVA, cocaine x $[Ca^{2+}]_o$ interaction; $F_{1, 12} = 4.72$, $P = 0.050$, $n = 4$), but
232 not at 10 ms or 100 ms IPI. These effects were not due to a potential electrochemical change in dopamine
233 adsorption/desorption kinetics at the electrode that might occur with a change in divalent cations, since
234 these effects of cocaine prevailed when the reduction in $[Ca^{2+}]_o$ was compensated by substitution with Mg^{2+}
235 (**Suppl. Fig. S6**)**.** Inhibition of the DAT therefore relieves a limiting clamp on a relationship between PPR and
236 initial release, suggesting that the DAT limits the release-dependence of short-term plasticity and drives STD.

237 ## The DAT maintains K^+-dependent gating of short-term plasticity

238 We noted that the effect of DAT inhibitors on STD resembled the effect of low $[K^+]_o$. Since inhibition of the
239 DAT might prevent DAT-mediated depolarising conductances and modify axonal hyperpolarisation/
240 repolarisation, we tested whether cocaine and low $[K^+]_o$ relieve STD via an overlapping mechanism. We
241 identified whether cocaine precluded the effect of varying $[K^+]_o$ (1 vs 5 mM) on short-term plasticity, in CPu
242 and NAc.

243 In CPu, in the absence of cocaine, PPR were elevated in lower $[K^+]_o$ (**Fig. 8A,B**, Two-way ANOVA, main
244 effect $[K^+]_o$, $F_{1, 18} = 20.47$, $P = 2.62 \times 10^{-4}$, $n = 4$) as seen in Fig. 3. Cocaine increased 1p-evoked peak $[DA]_o$ to a
245 similar extent in 5 mM versus 1 mM $[K^+]_o$ (**Fig. 8C**) but prevented the effect on PPR of varying $[K^+]_o$ (**Fig. 8D**,
246 Two-way ANOVA, $[K^+]_o$ x cocaine interaction, $F_{1, 12} = 7.686$, $P = 0.017$, $n = 8$). The limited ability of low $[K^+]_o$ to
247 increase PPR was not due to a ceiling effect (such as DA depletion due to increased 1p release); cocaine also
248 prevented the opposite effects of a rise in $[K^+]_o$ (to 7.5 mM) from decreasing PPR (**Suppl. Fig. S7**). In NAc, PPR
249 were slightly elevated in lower $[K^+]_o$ (**Fig. 8E,F**, Two-way ANOVA, main effect $[K^+]_o$, $F_{1,12} = 6.840$, $P = 0.023$, $n =$
250 3). Cocaine increased 1p-evoked peak $[DA]_o$ to a similar extent in 5 mM versus 1 mM $[K^+]_o$ (**Fig. 8G**), and, as in
251 CPu, prevented the effect of varying $[K^+]_o$ on PPR (**Fig. 8F,H**, Two-way ANOVA, $[K^+]_o$ x cocaine interaction, $F_{1,8}$
252 $= 6.756$, $P = 0.032$, $n = 3$). The effects of $[K^+]_o$ on short-term plasticity are therefore abolished by cocaine,
253 suggesting that short-term plasticity is regulated by a pathway common to $[K^+]_o$ and DAT function. DAT
254 function appears to regulate short-term plasticity by limiting Ca^{2+}-dependent gating whilst supporting $[K^+]_o$-
255 dependent modulation.

256 ## The DAT and K^+ regulate axonal activation

257 Finally, to validate that $[K^+]_o$ and the DAT are able to directly modulate the activation of DA axons, through
258 mechanisms upstream of vesicular P_r, we imaged Ca^{2+} dynamics in a population of DA axons in CPu using
259 genetically encoded calcium indicator GCaMP6f expressed in DAT-Cre:Ai95D mice (**Fig. 9A**). We activated DA
260 axons using the same single and paired stimulus pulses and conditions used to drive DA release, for two

261 representative IPIs of 10 and 40 ms. We noted firstly, in control conditions for each experiment, that axonal
262 Ca^{2+} levels evoked by 2p were significantly greater than those evoked by 1p, and were greater for IPIs of 10
263 ms than 40 ms (P<0.001, two-tailed paired t-test, n = 10) (**Fig. 9B-D**), which paralleled our observations of
264 evoked $[DA]_o$ throughout this study (e.g. see Fig. 1A,C). When we increased $[K^+]_o$ from 5 mM to 7.5 mM, Ca^{2+}
265 levels in DA axons evoked by paired pulses (normalised to 1p) were slightly but significantly decreased for
266 both IPI (**Fig**. 9B,C, Two-way ANOVA, main effect of $[K^+]_o$, $F_{1, 8}$ = 25.95, P =0.0009, N = 5 animals), consistent
267 with reduced re-activation of DA axons by a second pulse and the enhanced STD of DA release (see Fig. 3C).
268 Furthermore, when we inhibited DATs with cocaine (5 μM), we found that Ca^{2+} levels evoked in DA axons by
269 paired pulses were significantly modified, through a significant interaction between cocaine and IPI, which
270 significantly increased Ca^{2+} levels at IPI of 40 ms, to levels seen at 10 ms (**Fig 9D,E**, Two-way ANOVA,
271 interaction, $F_{1, 8}$ = 23.19, P = 0.0013, N = 5 animals). This interaction broadly paralleled the impact of DAT
272 inhibition on DA release at these IPIs (compare with Fig. 6A,B), and was consistent with a reduced STD in DA
273 release being due at least in part to elevated re-activation of DA axons in the absence of DAT action.

274 Discussion

275 We addressed whether the mechanisms that control the short-term dynamic probability of DA release, in
276 dorsal and ventral striatum, are governed by classic release-dependent or other release-independent
277 mechanisms. We show that short-term plasticity is governed in only a limited manner by Ca^{2+}-dependent
278 regulation of release probability, which participates in determining STF but not STD, and to greater extent in
279 ventral than dorsal striatum. We reveal that mechanisms insensitive to the initial level of release drive strong
280 STD, which is therefore not limited by the vesicular pool. Rather, we find that axonal excitability and the DAT
281 are major players in controlling STD, and they dominate over Ca^{2+}-dependent gating. The DAT appears to be
282 a master regulator that sets the dynamic level of DA release and its resulting STF, and clamps release leading
283 to release-insensitive STD particularly in dorsal striatum. The differences seen between dorsal and ventral
284 striatum could lead to divergent DA outputs in response to changes in action potential firing and to striatal
285 modulatory inputs.

286 ## Calcium-dependent facilitation

287 Studies of short-term plasticity at fast central synapses typically demonstrate an inverse relationship
288 between PPR and initial P_r; STF is observed when P_r is low, and STD when P_r is high [47]. Here, we show that,
289 in NAc, an inverse relationship between STF and initial DA release could be observed for only short IPI
290 corresponding to instantaneous frequencies seen during fast burst firing (≥25 Hz), but the STD seen at lower
291 frequencies did not vary with initial release. By contrast, in CPu, there is limited relationship between Ca^{2+}-
292 limited initial release and the dynamic subsequent plasticity of DA release. Here, other release-independent
293 mechanisms seem particularly influential. Given this overall apparent divergence from mechanisms typically
294 operating at classic fast synapses, it is notable that some aspects of the molecular machinery supporting
295 presynaptic active zones for DA release also diverge from that supporting fast synapses (e.g. RIM- and ELKS-
296 dependence) [17].

297 STF at other synapses is often attributed to summation of residual Ca^{2+} [48,49], or Ca^{2+}-dependent
298 ultrafast recruitment of vesicles [50]. Ca^{2+} dynamics can vary with local Ca^{2+} buffering mechanisms [51]. In
299 NAc, we saw a more pronounced Ca^{2+}-dependent STF than in CPu, despite a weaker relationship between
300 $[Ca^{2+}]_o$ and initial DA release in NAc. These regional differences might correspond to differences in Ca^{2+}
301 binding proteins. For example, the high-affinity fast Ca^{2+} buffer calbindin-D_{28k} is expressed at 2-3-fold greater
302 levels in DA neurons of ventral tegmental area (VTA) which more strongly innervate NAc than neurons of
303 substantia nigra pars compacta (SNc) which more strongly innervate CPu [52-54]. Calbindin might provide
304 extra initial Ca^{2+} buffering capacity to limit initial release in NAc, but become saturated at subsequent
305 stimuli, which in other neurons promotes STF [55,56].

306 ## Release-insensitive depression

307 At longer interpulse intervals (40-200 ms) corresponding to a range of physiological firing frequencies (5-25
308 Hz), there is strong STD of DA release. This is not due to D_2 autoreceptor (D2R) activation at these intervals.
309 STD of release of other transmitters can result from depletion of readily-releasable vesicles [57], but the STD

310 in DA release does not seem to result from a limited availability of DA vesicles. Not only is a low fraction of
311 presynaptic DA estimated to be released after stimulation [14,17,58,59], but moreover STD in the present
312 study was not relieved by reducing initial release (by lowering $[Ca^{2+}]_o$). Ca^{2+}-dependent inactivation of VGCCs
313 by a Ca^{2+} sensor has also been proposed at some central synapses [60-62] but since low $[Ca^{2+}]_o$ did not
314 relieve STD for DA release, this mechanism is unlikely to contribute here.

315 Since STD of DA release is not sensitive to the magnitude of initial release, it appears to be a release-
316 insensitive depression. We found particularly in CPu, that STD varied with $[K^+]_o$, as seen at some other
317 central synapses [63]. The variation in STD despite no change in initial release further demonstrate the
318 uncoupling of STD from P_r. The effects of $[K^+]_o$ suggested that factors underpinning the ability to re-activate
319 DA axons, such as membrane polarity/excitability, are critical in determining STD for DA release. Using Ca^{2+}
320 imaging, we validated that changes in $[K^+]_o$ modify the ability to activate DA axons at subsequent stimuli,
321 consistent with axonal excitability being a critical factor in STD of DA release, upstream of local regulation of
322 vesicular P_r. A range of K_v channel classes can regulate axonal excitability and rates of repolarisation in CNS
323 axons [64-67]. Varying $[K^+]_o$ would be expected to change the Nernstian driving force for active K^+ currents
324 [42], altering action potential waveform and repolarisation and therefore the degree of Na^+ channel
325 inactivation, or alternatively might alter the rate of K^+ channel inactivation [43], leading to use-dependent
326 changes in membrane potential which alter Na^+ channel recruitment at a second pulse. We cannot
327 distinguish here which of these opposing mechanisms dominates to govern short-term plasticity but in either
328 scenario, Na^+-channel recruitment would be altered.

329 The critical role for axonal excitability in DA STD is particularly pertinent given DA axon morphology.
330 Midbrain DA neurons form small diameter, unmyelinated, extensively arborised axons each containing on
331 the order of ~10^4 branch points [20,68]. These morphological features will not readily favour reliable
332 conduction of action potentials [69]. K^+ or Na^+ conductances are very influential in axonal conduction
333 [63,70,71] and are likely to influence the fidelity or failure of action potential propagation through the DA
334 axonal tree. Action potential properties and propagation failure could be key contributors to DA STD. As a

335 consequence, the size of the DA axonal arbour invaded and the striatal field modulated by DA could be
336 dynamically adapted by presynaptic activity and locally by neuromodulatory inputs. In this regard, it is
337 noteworthy that nAChRs regulate DA release and can drive a strong STD that limits the frequency sensitivity
338 in DA signals [11,15]. ACh input to nAChRs might play a strategic role in shaping action potential propagation
339 and fidelity throughout the axonal arbour.

340 Changes in propagation fidelity would be expected to have a greater impact on release where axonal
341 arbours are more extensive. Notably, the axonal arbours formed by DA neurons projecting to CPu are more
342 extensive than those projecting to NAc [19,20,72]. In parallel, short-term plasticity showed stronger
343 dependence on K^+-dependent gating in CPu than in NAc. This correlation suggests that action potentials in
344 VTA DA neurons might more readily invade a fuller extent of their axonal tree than action potentials in SNc
345 DA neurons, a speculation which could be tested in future studies with significant implications for signal
346 processing by these neurons.

347 Together, these findings suggest that Ca^{2+} -dependent mechanisms can modify amplitude of DA
348 signals, but will not change the dynamic contrast in DA signals when DA neurons change their firing
349 frequency, except at very highest frequencies in NAc. Conversely, mechanisms that modulate the driving
350 forces on membrane potential and repolarisation, will particularly influence the dynamic contrast in DA
351 signals.

352 Role of the DAT in short-term plasticity

353 The DAT in striatum is known to regulate DA transmission through several means. DATs can curtail the
354 extracellular summation and lifetime of $[DA]_o$ through re-uptake [73], and can also limit the DA release
355 process [29-32]. Correspondingly, we show firstly that DAT function promotes STF of DA release at short
356 interpulse intervals (10 ms in CPu, and up to 25 ms in NAc) when short-term plasticity of DA release co-varies
357 most strongly with initial release (see Fig. 1). But secondly, at longer intervals, corresponding to typical firing
358 frequencies (5-25 Hz), when release is dominated by release-independent depression, we found that the

359 DAT promotes STD, particularly in CPu. DAT function therefore can therefore promote both STF and STD.
360 These effects are akin to changing both Ca^{2+}-dependent P_r and K^+-dependent excitability, but neither in
361 isolation, and therefore indicate that the DAT is limiting initial DA release probability and also subsequent
362 release through likely polarisation-dependent mechanisms.

363 The effects of DAT inhibition on STF at short IPIs seemed large given that, under control conditions,
364 the relationship between initial release and STF was weak. This disparity is reconciled by our finding that DAT
365 inhibition permitted Ca^{2+}-dependent modulation of short-term plasticity, suggesting that the DAT is a critical
366 player that controls and limits the relationship between Ca^{2+} and release probability. The mechanisms are
367 not yet known. DATs have previously been suggested to inhibit Ca^{2+}-dependent vesicle mobilisation via
368 interactions with synapsins, with synapsin-3 indicated as a potential candidate [29,30]. But our data with
369 synapse-3 KOs do not readily support a synapsin3-dependent inhibition of vesicle recruitment by the DAT.
370 The DAT is also an electrogenic transporter [74,75] that mediates a depolarising current [27,28,45] and can
371 interact directly with VGCCs [76] which might influence depolarization-dependent Ca^{2+} dynamics in DA
372 axons. However, Ca^{2+} imaging in DA axons in CPu did not reveal an impact of DAT inhibition on Ca^{2+} levels for
373 paired pulses at very short IPIs where STF occurs, suggesting that the impact of DATs on STF at very short
374 intervals seems to be downstream of Ca^{2+} entry, e.g. in the mobilisation of vesicle pool or local regulation of
375 vesicular P_r. There might be redundancy within the synapsin family to continue to support a synapsin-
376 dependent mechanism in the absence of synapsin3.

377 The DAT, like $[K^+]_o$, also acted to promote depression at longer, physiological IPIs (40 – 200 ms). The
378 overlap between the effects on STD of the DAT, $[K^+]_o$ and K_v channel inhibitors suggested that the DAT acts
379 through mechanisms that govern axonal activation. Using Ca^{2+} imaging we validated that DATs indeed limit
380 the ability to activate DA axons at subsequent stimuli at these intervals. Thus, DATs might act to attenuate
381 propagation of subsequent action potentials through the DA axon arbour. Since hyperpolarisation and low
382 $[K^+]_o$ can promote action potential renewal and propagation in some axon types [77], the potential for the
383 DAT, like high $[K^+]_o$, to depolarise membrane potential [27,28] might contribute to poor axonal re-activation

384 in DA axons. It is of note that DATs are widely distributed throughout the length of DA axons [78], and are
385 found at locations thought to correspond to both release-active zones and inactive zones [17]. DAT function
386 can also be modulated by DA D2 and D3-receptors [79,80]. DATs could be ideally positioned to govern action
387 potential propagation on axons and at branches, action potential waveform at release active zones (e.g. [66])
388 and/or the recruitment of vesicles or VGCCs at active zones, modulated by DA. The higher density of DA in
389 dorsolateral striatum, and greater DAT transcript levels in SNc than VTA neurons [54], could lead to stronger
390 limitations on action potential waveforms in CPu than NAc. Now defined, these hypotheses should be tested
391 directly in future studies.

392 It is well known that DAT function can promote the frequency-dependence of DA release during
393 ongoing activity [25,31,33,81,82]. These effects are consistent with the effects of uptake on extracellular
394 summation between stimuli and also with the role of DAT in the dynamic probability of release we have
395 identified here. The DAT might then determine both the fidelity and the spatial range of striatal DA
396 transmission not only through its established roles in limiting DA diffusion, but also, by limiting the
397 probability of DA release and activation of the axonal arbour.

398 In conclusion, we propose a hierarchy of intrinsic mechanisms that control short-term plasticity of
399 DA release. Within this hierarchy, the DAT represents a 'master regulator', governing the balance between
400 release-dependent and release-independent mechanisms that differently dominate in dorsal versus ventral
401 striatum. In turn, DAT inhibitors such as cocaine will have profound effects on DA signalling through
402 promoting P_r, relieving STD, and altering the timecourse and spatial field of DA signals.

403 Materials and Methods

404 **Animals**

405 Experiments were carried out using adult male C57Bl6/J mice (Jackson Laboratories), heterozygous DAT^{IRES}-
406 ^{Cre} mice, synapsin-III knockout (S3KO) mice, or DAT-Cre:Ai95D mice on a C57Bl6/J background. For

407 experiments using optical stimulation of DA axons, male heterozygote DAT-internal ribosome entry site
408 (IRES)-Cre mice were bred from homozygous DAT$^{IRES\text{-}Cre}$ mice on a C57Bl6/J background (B6.SJL-
409 Slc6$^{a3tm1.1(cre)Bkmn}$/J, stock # 006660, Jackson Laboratories). S3KO mice were bred as described previously
410 (Feng et al., 2002), and were kindly supplied by Professor HT Kao (Brown University). For Ca^{2+} imaging
411 experiments, male heterozygous DAT-Cre:Ai95D mice (4 -8 weeks) were bred from homozygous DAT-Cre
412 mice (B6.SJL-Slc6$^{a3tm1.1(cre)Bkmn}$/J, JAX stock number 006660) crossed with homozygous Ai95D mice (B6;129S-
413 Gt(ROSA)26Sor$^{tm95.1(CAG\text{-}GCaMP6f)Hze}$/J, JAX stock number 028865). Animals were group-housed and maintained
414 on a 12-hr light/dark cycle with *ad libitum* access to food and water. All procedures were performed in
415 accordance with the Animals in Scientific Procedures Act 1986 (Amended 2012) with ethical approval from
416 the University of Oxford, and under authority of a Project Licence granted by the UK Home Office.

417 **Surgery**

418 Heterozygote DAT$^{IRES\text{-}Cre}$ mice were injected intracerebrally with a Cre-inducible recombinant AAV serotype 5
419 vector containing an inverted gene for channelrhodopsin-2 fused in-frame with a gene encoding enhanced
420 yellow fluorescent protein (pAAV-double floxed-hChR2(H134R)-EYFP-WPRE-pA), as we have used previously
421 [11]. Mice were placed in a stereotaxic frame under isoflurane anaesthesia and a craniotomy was made above
422 the injection site. Injections of 1 µL virus were given either unilaterally or bilaterally in either VTA (co-ordinates
423 from Bregma in mm: AP -3.1, ML ±0.5, DV -4.4) or in the SNc (from Bregma in mm: AP -3.5, ML ±1.2, DV -4.0)
424 using a 2.5 µL 33-gauge Hamilton syringe at 0.2 µL/min with a microinjector. The syringe was left in place for
425 10 minutes following each injection, then retracted slowly. Animals were maintained for at least 3 weeks
426 following surgery to allow virus expression in striatum.

427 **Slice Preparation**

428 Striatal slices were prepared as described previously [83,84]. Mice were sacrificed by cervical dislocation and
429 the brains removed and transferred to ice-cold HEPES-based buffer containing in mM: 120 NaCl, 20 $NaHCO_3$,
430 6.7 HEPES acid, 5 KCl, 3.3 HEPES salt, 2 $CaCl_2$, 2 $MgSO_4$, 1.2 KH_2PO_4, 10 glucose, saturated with 95%O_2/5%CO_2.
431 Acute 300 µm thick coronal striatal slices, containing both dorsal striatum (CPu) and nucleus accumbens core
432 (NAc) were prepared in ice-cold HEPES-based buffer and cut using a vibratome (VT1000S or VT1200S; Leica).

433 Slices were kept at room temperature in HEPES-based buffer for 1 hour before being transferred to the
434 recording chamber and superfused at 1.8-2.0 ml/min in bicarbonate buffer-based artificial CSF (aCSF)
435 containing in mM: 124.3 NaCl, 26 $NaHCO_3$, 3.8 KCl, 2.4 $CaCl_2$, 1.3 $MgSO_4$, 1.2 KH_2PO_4, 10 glucose, saturated
436 with 95% O_2/5% CO_2, at 31-33°C. Recording medium also contained dihydro-β-erythroidine (DHβE, 1 μM), an
437 antagonist of β2 subunit-containing nAChRs. Slices were allowed to equilibrate for 30 minutes prior to
438 recording.

439 **Voltammetry and Stimulation**

440 Evoked extracellular DA concentration ($[DA]_o$) was measured using FCV at carbon-fibre microelectrodes (fibre
441 diameter 7-10 μm, tip length 50-100 μm) implanted to a constant depth of 100 μm. A triangular voltage
442 waveform was scanned across the microelectrode (-700 to +1300 mV and back vs Ag/AgCl reference, scan rate
443 800 V/s) using a Millar voltammeter (Julian Millar, Barts and the London School of Medicine and Dentistry),
444 with a sweep frequency of 8 Hz, as described previously [83]. This sampling rate is sufficient to capture the
445 rising and falling phase of the DA transients; faster sampling rates do not change the data interpretations (not
446 illustrated). Evoked currents were confirmed as DA by comparison of the voltammogram with that produced
447 during calibration with applied DA in aCSF (oxidation peak +500-600 mV and reduction peak -200 mV). Currents
448 at the oxidation peak potential were measured from the baseline of each voltammogram and plotted against
449 time to provide profiles of $[DA]_o$ versus time. Electrodes responded linearly to $[DA]_o$ over the concentration
450 range detected. Electrodes were calibrated after use in 2 μM DA in each experimental solution used, including
451 all solutions where $[Ca^{2+}]$ was varied, since electrode sensitivity varies with divalent ion concentration [85].
452 Calibration solutions were made up immediately before use from stock solution of 2.5 mM DA in 0.1 M $HClO_4$
453 stored at 4°C. Electrode sensitivities ranged from 5-25 nA/μM.

454 For experiments using electrical stimulation, DA release was evoked using a surface bipolar concentric
455 Pt/Ir electrode (25 μm diameter, FHC) placed approximately 100 μm from the recording electrode. Stimulation
456 pulses of 200 μs duration were applied at 0.6 mA unless described otherwise.

457 For optogenetic stimulation, DA release was evoked in striata from $DAT^{IRES\text{-}Cre}$ mice conditionally
458 expressing ChR2 in DA axons, using 2 ms full-field illumination from an LED system emitting light at 470 nm

459 wavelength (OptoLED, Cairn Research) as described previously [11]. The LED system illuminated an area of 2.2
460 mm diameter. The current delivered by the LED power supply was set to produce a perimaximal light intensity
461 (i.e. the minimum light intensity able to evoke maximum $[DA]_o$ following a single 2 ms pulse). Since the
462 perimaximal light intensity is dependent on the level of ChR2 expression, which varies between animals, the
463 appropriate current was determined at the beginning of each experiment. Electrical or optical stimulations
464 were delivered every 2.5 minutes, after which dopamine release was reproducible. Before acquisition of
465 experimental data, peak evoked $[DA]_o$ levels were allowed to reach this reproducible stable level.

466 All experiments were conducted in the presence of nAChR antagonist DHβE (1 μM) to prevent
467 confounding effects of striatal ACh. Striatal nAChRs operate a profound control over striatal DA release: ACh
468 released by striatal stimulation can directly drive axonal DA release [11] and limit dependence of DA release
469 on presynaptic frequency [15,83] which can mask other mechanisms operating presynaptically on DA axons.
470 Inclusion of nAChR antagonists during local stimulation also makes evoked DA release in *ex vivo* slice sensitive
471 to frequency of stimulation [15,83] as seen *in vivo* after midbrain or medial forebrain bundle stimulation
472 [81,86].

473 **DA release study design and analyses**

474 The term release probability P_r used for DA here is a composite measure of synaptic P_r (a function of
475 vesicular P_r and the size of the pool of vesicles) and the number of release sites and fibres recruited by the
476 stimulus. Short-term plasticity in DA release was explored by applying alternating single pulses (1p) or paired
477 pulses (2p) with inter-pulse intervals (IPIs) of 10 ms – 200 ms in pseudorandom order and in triplicate at each
478 recording site. IPIs of 40 to 200 ms fall within the range commonly observed during burst firing in DA
479 neurons *in vivo* [3,4]. IPIs of 10 to 25 ms have been observed during burst firing in rat DA neurons [4] but are
480 particularly useful to interrogate short-term facilitation which occurs on this timescale [15,25].

481 We calculated paired-pulse ratio (PPR) as a measure of short-term plasticity. We define PPR as the
482 ratio P2/P1, where P1 is peak $[DA]_o$ detected following 1p stimulus and P2 is the peak $[DA]_o$ attributable to
483 the second stimulation only. P2 was determined by subtracting the entire $[DA]_o$ transient including decay
484 phase after a single pulse from the summated paired-pulse response, and we therefore account for

485 summation and decay resulting from uptake kinetics. Any enhanced spillover resulting from uptake
486 inhibition will occur for single and paired pulses and should therefore be controlled for. We cannot control
487 for variable fiber recruitment for different stimuli, but can control for variable modulation by other local
488 inputs: PPR on the timecourses explored here is not differently modified at different intervals by D2
489 dopamine receptors (see Results), or by GABA receptors (Lopes and Cragg, unpublished observations). We
490 use the term "release-dependent" plasticity to indicate a relationship between PPR and P1 $[DA]_o$. "Release-
491 insensitive" or "release-independent" refers to a PPR that varies independently of P1, or does not vary with
492 P1.

493 Calcium concentration ($[Ca^{2+}]_o$) in aCSF was varied by varying $[CaCl_2]$. In some experiments where
494 stated, a reduction in $CaCl_2$ was substituted with $MgCl_2$. However, Ca^{2+}/Mg^{2+} substitution was not routine
495 because other effects of $[Mg^{2+}]_o$ can confound interpretation. Changes in $[Mg^{2+}]$ have been shown to alter
496 Ca^{2+} currents through VGCCs [87,88], alter G-protein-coupled receptor function, including dopamine D2
497 receptors [89], change the affinity of calcium-binding protein calbindin for Ca^{2+} [90], trigger complexing of
498 Ca^{2+} by ATP [91], and alter the sensitivity of FCV electrodes to DA [85], and we find also that Ca^{2+}/Mg^{2+}
499 substitution reduces DA release to levels below those of reducing Ca^{2+} alone (**Supplementary Figure S6D**).

500 Where extracellular potassium concentration ($[K^+]_o$) was varied (1.0 - 7.5 mM), changes in osmolarity
501 were corrected by varying $[Na^+]$. The Na^+- and K^+-containing salts present in aCSF were varied as follows (in
502 mM): In experiments with 1 mM $[K^+]_o$, salts were 127.1 NaCl, 1.0 KCl, 0 KH_2PO_4, 1.2 NaH_2PO_4; For 1.25 mM
503 $[K^+]_o$ salts were 128.0 NaCl, 0.05 KCl, 1.2 KH_2PO_4; For 7.5 mM $[K^+]_o$, salts were 121.8 NaCl, 6.3 KCl and 1.2
504 KH_2PO_4. Recordings in control conditions were collected before and after each experimental manipulation at
505 each recording site. Slices were equilibrated in each solution for at least 20 minutes before data were
506 included for analysis. Experiments were carried out in either the dorsal half of the caudate-putamen (CPu)
507 (dorsolateral and dorsomedial striatum) or nucleus accumbens core (NAc) (within 200 μm of the anterior
508 commissure), one site per slice. Release is TTX-sensitive [11]. Manipulations of $[Ca^{2+}]_o$ or $[K^+]_o$ did not change
509 DA decay rates.

510 Data were acquired and analysed using Axoscope 10.2, 10.5 (Molecular Devices) or Strathclyde
511 Whole Cell Program (University of Strathclyde, Glasgow, UK) and locally-written scripts in Visual Basic for
512 Applications (Microsoft). Data are expressed as mean ± standard error (SEM) and *n* = number of animals (the
513 number of different biological replicates). Each experiment was performed at a single recording site in one
514 brain slice. Within a given experiment at each single recording site, technical replicates were usually
515 obtained in at least triplicate before averaging to obtain the value for that experiment at that recording site.
516 Statistical comparisons were carried out using GraphPad Prism 6, 7 and 8 (GraphPad Software Inc.) using
517 ANOVAs, post-hoc two-tailed t-tests with n = number of animals. Data were tested for normality before
518 using parametric tests.

519 **Ca^{2+} imaging**

520 An Olympus BX51Wl microscope equipped with a CAIRN Research OptoLED Lite system, Prime Scientific CMOS
521 (sCMOS) Camera (Teledyne Photometrics), and a 40x/0.8 NA water-objective (Olympus) was used for wide-
522 field fluorescence imaging of GCaMP6f in dopaminergic axons in dorsolateral CPu in *ex vivo* slices in response
523 to single and paired electrical stimulus pulses. Images were acquired at 16.6 Hz frame rate every 2.5 minutes
524 using Micro-Manager 1.4, with stimulation and recording synchronised using custom-written procedures in
525 Igor Pro 6 (WaveMetrics) and an ITC-18 A/D board (Instrutech). Image files were analysed with Matlab R2017b
526 and Fiji 1.5. We extracted fluorescence intensity from the region of interest (ROI) and from an equal
527 background area where there was no GCaMP6f expression (on the stimulating electrode). After background
528 subtraction, the Ca^{2+} transients were bleach-corrected by fitting an exponential curve function through both
529 the baseline (2 s prior to stimulation) and the last 1 s in a 7.2 s recording window. Data are expressed as ΔF/F
530 where F is the fitted curve. The order of single and paired stimulation pulses was alternated and equally
531 distributed, and data were collected in duplicate before and after a change in extracellular experimental
532 condition. Data are expressed as mean ± standard error of the mean (SEM) for each stimulus condition. N
533 value is the number of animals. Statistical analyses used GraphPad Prism 7.03, for two-way ANOVA with post-
534 hoc t-tests. All experiments were conducted in the presence of DHβE (1 μM). GCaMP6f responses were
535 quantified as the mean ΔF/F value.

536 **Immunocytochemistry**

537 We verified the specificity of GCaMP6f expression to dopaminergic structures by comparing direct eGFP
538 fluorescence to immunoreactivity to tyrosine hydroxylase (TH-ir). Acute slices of midbrain and striatum were
539 fixed overnight at 4 ^{o}C in 4% paraformaldehyde dissolved in PBS, then stored in PBS. After resectioning to 40
540 µm, free-floating sections were washed in PBS 5 x 5 min and incubated in 0.5% Triton X-100, 10% normal
541 goat serum and 10% fetal bovine serum for 30 min. Slices were subsequently incubated overnight with
542 1:2000 primary (rabbit anti-TH; Sigma) antibody dissolved in PBS containing 0.5% Triton X-100, 1% normal
543 goat serum and 1% fetal bovine serum. Sections were then washed with PBS 5 x 5 min and incubated for 2 hr
544 at room temperature with 1:1000 secondary (DyLight 594 goat anti-rabbit; Jackson) antibody dissolved in
545 PBS containing 0.5% Triton X-100, 1% normal goat serum and 1% fetal bovine serum. Sections were washed
546 with PBS and mounted on gelled slides with Vectashield mounting medium (Vector Labs) and imaged using a
547 Zeiss LSM880 (confocal) running Zen black version 2.3, at 20x, N.A. 0.8. Maximum intensity projection from a
548 z-stack of height 30 µm was captured individually and the stack of the pictures were compressed. TH (red)
549 was captured at 638-759 nm with 633 nm excitation light. GCaMP (green) was excited with 488 nm and
550 captured at 493-630 nm.

551 **Drugs**

552 DHβE and lidocaine were obtained from Tocris Biosciences or Ascent Scientific. Cocaine hydrochloride and
553 nomifensine maleate were obtained from Sigma. Methylphenidate (Ritalin™) was obtained from Novartis. All
554 drugs were dissolved in either de-ionised water, aqueous acid (nomifensine maleate) or ethanol (lidocaine)
555 to make stock aliquots at 1000-10,000x final concentration and stored at -20 ^{o}C prior to use. DA uptake
556 inhibitors were used at standard concentrations that have detectable outcomes on uptake kinetics
557 concentrations but are lower than those that lead to run-down of release and/or have non-selective effects
558 as local anaesthetics or at nAChRs [46,92,93].

559 **Acknowledgements:** Funding sources: MRC, BBSRC Interdisciplinary Doctoral Training Program, Clarendon
560 Fund, Monument Trust Parkinson's UK Discovery Award, and Christ Church Oxford.

Author contributions: M.D.C. designed and performed experiments, analysed and interpreted the data, and co-wrote the manuscript. N.J.P. designed and performed experiments, and analysed and interpreted the data. B.M.R, S.V.M. and M.Y.T performed experiments and analysed data. K.R.B., S.T. and S.J.C. supervised the work. S.J.C. designed the experiments, interpreted the data, and co-wrote the manuscript.

Declaration of Interests: The authors declare no competing interests.

Data Availability

The authors declare that all data sets generated and analysed during this study are available within this paper and its supplementary files. The source data underlying all figures and supplementary figures are provided as a Source Data file.

570 ## References

571 1. Cohen JY, Haesler S, Vong L, Lowell BB, Uchida N (2012). Neuron-type-specific signals for reward and
572 punishment in the ventral tegmental area. *Nature* 482:85-88.

573 2. Grace AA, Bunney BS (1984). The control of firing pattern in nigral dopamine neurons: single spike
574 firing. *J Neurosci* 4:2866-2876.

575 3. Grace AA, Bunney BS (1984). The control of firing pattern in nigral dopamine neurons: burst firing. *J*
576 *Neurosci* 4:2877-2890.

577 4. Hyland BI, Reynolds JNJ, Hay J, Perk CG, Miller R (2002). Firing modes of midbrain dopamine cells in
578 the freely moving rat. *Neuroscience* 114:475-492.

579 5. Pan WX, Schmidt R, Wickens JR, Hyland BI (2005). Dopamine Cells Respond to Predicted Events during
580 Classical Conditioning: Evidence for Eligibility Traces in the Reward-Learning Network. *J Neurosci*
581 25:6235-6242.

582 6. Jin X, Costa RM (2010). Start/stop signals emerge in nigrostriatal circuits during sequence learning.
583 *Nature* 466:457-462.

584 7. Matsumoto M, Hikosaka O (2009). Two types of dopamine neuron distinctly convey positive and
585 negative motivational signals. *Nature* 459:837-841.

586 8. Schultz W (1986). Responses of midbrain dopamine neurons to behavioral trigger stimuli in the
587 monkey. *J Neurophysiol* 56:1439-1461.

588 9. Sulzer D, Cragg SJ, Rice ME (2016). Striatal dopamine neurotransmission: Regulation of release and
589 uptake. *Basal Ganglia* 6:123-148.

590 10. Hamid AA, Pettibone JR, Mabrouk OS, Hetrick VL, Schmidt R, Vander Weele CM, Kennedy RT, Aragona
591 BJ, Berke JD (2016). Mesolimbic dopamine signals the value of work. *Nat Neurosci* 19:117-126.

592 11. Threlfell S, Lalic T, Platt NJ, Jennings KA, Deisseroth K, Cragg SJ (2012). Striatal dopamine release is
593 triggered by synchronized activity in cholinergic interneurons. *Neuron* 75:58-64.

594 12. Cachope R, Mateo Y, Mathur BN, Irving J, Wang HL, Morales M, Lovinger DM, Cheer JF (2012).
595 Selective activation of cholinergic interneurons enhances accumbal phasic dopamine release: setting
596 the tone for reward processing. *Cell Rep.* 2:33-41.

597 13. Mohebi A, Pettibone JR, Hamid AA, Wong JT, Vinson LT, Patriarchi T, Tian L, Kennedy RT, Berke JD
598 (2019). Dissociable dopamine dynamics for learning and motivation. *Nature* 570:65-70.

599 14. Cragg SJ (2003). Variable dopamine release probability and short-term plasticity between functional
600 domains of the primate striatum. *J Neurosci* 23:4378-4385.

601 15. Rice ME, Cragg SJ (2004). Nicotine amplifies reward-related dopamine signals in striatum. *Nat Neurosci*
602 7:583-584.

603 16. Montague PR, McClure SM, Baldwin PR, Phillips PEM, Budygin EA, Stuber GD, Kilpatrick MR, Wightman
604 RM (2004). Dynamic gain control of dopamine delivery in freely moving animals. *J Neurosci* 24:1754-
605 1759.

606 17. Liu C, Kershberg L, Wang J, Schneeberger S, Kaeser PS (2018). Dopamine Secretion Is Mediated by
607 Sparse Active Zone-like Release Sites. *Cell* 172:706-718.e15.

608 18. Debanne D (2004). Information processing in the axon. *Nature Rev Neurosci* 5:304-316.

609 19. Aransay A, Rodríguez-López C, García-Amado M, Clascá F, Prensa L (2015). Long-range projection
610 neurons of the mouse ventral tegmental area: a single-cell axon tracing analysis. *Front Neuroanat*
611 9:59.

612 20. Matsuda W, Furuta T, Nakamura KC, Hioki H, Fujiyama F, Arai R, Kaneko T (2009). Single nigrostriatal
613 dopaminergic neurons form widely spread and highly dense axonal arborizations in the neostriatum. *J*
614 *Neurosci* 29:444-453.

615 21. Pissadaki EK, Bolam JP (2013). The energy cost of action potential propagation in dopamine neurons:
616 clues to susceptibility in Parkinson's disease. *Front Comput Neurosci* 7:13.

617 22. Collins AL, Aitken TJ, Greenfield VY, Ostlund SB, Wassum KM (2016). Nucleus Accumbens Acetylcholine
618 Receptors Modulate Dopamine and Motivation. *Neuropsychopharmacol* 41:2830-2838.

619 23. Zhang H, Sulzer D (2004). Frequency-dependent modulation of dopamine release by nicotine. *Nat*
620 *Neurosci* 7:581-582.

621 24. Wang L, Shang S, Kang X, Teng S, Zhu F, Liu B, Wu Q, Li M, Liu W, Xu H, Zhou L, Jiao R, Dou H, Zuo P,
622 Zhang X, Zheng L, Wang S, Wang C, Zhou Z (2014). Modulation of dopamine release in the striatum by
623 physiologically relevant levels of nicotine. *Nat Commun* 5:3925.

624 25. Jennings KA, Platt NJ, Cragg SJ (2015). The impact of a parkinsonian lesion on dynamic striatal
625 dopamine transmission depends on nicotinic receptor activation. *Neurobiol Dis* 82:262-268.

626 26. Brimblecombe KR, Gracie CJ, Platt NJ, Cragg SJ (2015). Gating of dopamine transmission by calcium
627 and axonal N-, Q-, T- and L-type voltage-gated calcium channels differs between striatal domains. *J*
628 *Physiol* 593:929-946.

629 27. Carvelli L, McDonald PW, Blakely RD, Defelice LJ (2004). Dopamine transporters depolarize neurons by
630 a channel mechanism. *Proc Natl Acad Sci USA* 101:16046-16051.

631 28. Ingram SL, Prasad BM, Amara SG (2002). Dopamine transporter-mediated conductances increase
632 excitability of midbrain dopamine neurons. *Nat Neurosci* 5:971-978.

633 29. Kile BM, Guillot TS, Venton BJ, Wetsel WC, Augustine GJ, Wightman RM (2010). Synapsins differentially
634 control dopamine and serotonin release. *J Neurosci* 30:9762-9770.

635 30. Venton BJ, Seipel AT, Phillips PEM, Wetsel WC, Gitler D, Greengard P, Augustine GJ, Wightman RM
636 (2006). Cocaine Increases Dopamine Release by Mobilization of a Synapsin-Dependent Reserve Pool.
637 *Journal of Neuroscience* 26:3206-3209.

638 31. Daberkow DP, Brown HD, Bunner KD, Kraniotis SA, Doellman MA, Ragozzino ME, Garris PA, Roitman
639 MF (2013). Amphetamine paradoxically augments exocytotic dopamine release and phasic dopamine
640 signals. *J Neurosci* 33:452-463.

641 32. Hoffman AF, Spivak CE, Lupica CR (2016). Enhanced Dopamine Release by Dopamine Transport
642 Inhibitors Described by a Restricted Diffusion Model and Fast-Scan Cyclic Voltammetry. *ACS Chem*
643 *Neurosci* 7:700-709.

644 33. Zhang L, Doyon WM, Clark JJ, Phillips PEM, Dani JA (2009). Controls of Tonic and Phasic Dopamine
645 Transmission in the Dorsal and Ventral Striatum. *Molec Pharmacol* 76:396-404.

646 34. Debanne D, Guérineau NC, Gähwiler BH, Thompson SM (1996). Paired-pulse facilitation and
647 depression at unitary synapses in rat hippocampus: quantal fluctuation affects subsequent release. *J*
648 *Physiol* 491:163-176.

649 35. Dobrunz LE, Stevens CF (1997). Heterogeneity of Release Probability, Facilitation, and Depletion at
650 Central Synapses. *Neuron* 18:995-1008.

651 36. Thomson AM (2000). Molecular frequency filters at central synapses. *Prog Neurobiol* 62:159-196.

652 37. Wilcox KS, Dichter MA (1994). Paired pulse depression in cultured hippocampal neurons is due to a
653 presynaptic mechanism independent of GABAB autoreceptor activation. *J Neurosci* 14:1775-1788.

654 38. Fisher SA, Fischer TM, Carew TJ (1997). Multiple overlapping processes underlying short-term synaptic
655 enhancement. *Trends Neurosci* 20:170-177.

656 39. Benoit-Marand M, Borrelli E, Gonon F (2001). Inhibition of dopamine release via presynaptic D2
657 receptors: time course and functional characteristics in vivo. *J Neurosci* 21:9134-9141.

658 40. Phillips PEM, Hancock PJ, Stamford JA (2002). Time window of autoreceptor-mediated inhibition of
659 limbic and striatal dopamine release. *Synapse* 44:15-22.

660 41. Schmitz Y, Schmauss C, Sulzer D (2002). Altered dopamine release and uptake kinetics in mice lacking
661 D2 receptors. *J Neurosci* 22:8002-8009.

662 42. Balestrino M, Aitken PG, Somjen GG (1986). The effects of moderate changes of extracellular K+ and
663 Ca2+ on synaptic and neural function in the CA1 region of the hippocampal slice. *Brain Res* 377:229-
664 239.

665 43. Baukrowitz T, Yellen G (1995). Modulation of K+ current by frequency and external [K+]: A tale of two
666 inactivation mechanisms. *Neuron* 15:951-960.

667 44. Nedergaard S (1999). Regulation of action potential size and excitability in substantia nigra compacta
668 neurons: sensitivity to 4-aminopyridine. *J Neurophysiol* 82:2903-2913.

669 45. Sonders MS, Zhu S-J, Zahniser NR, Kavanaugh MP, Amara SG (1997). Multiple Ionic Conductances of
670 the Human Dopamine Transporter: The Actions of Dopamine and Psychostimulants. *J Neurosci* 17:960-
671 974.

672 46. Acevedo-Rodriguez A, Zhang L, Zhou F, Gong S, Gu H, De Biasi M, Zhou F-M, Dani JA (2014). Cocaine
673 inhibition of nicotinic acetylcholine receptors influences dopamine release. *Front Synaptic Neurosci*
674 6:19.

675 47. Zucker RS, Regehr WG (2002). Short-term synaptic plasticity. *Ann Review Physiol* 64:355-405.

676 48. Chen C, Regehr WG (1999). Contributions of residual calcium to fast synaptic transmission. *J Neurosci*
677 19:6257-6266.

678 49. Katz B, Miledi R (1968). The role of calcium in neuromuscular facilitation. *J Physiol* 195:481-492.

679 50. Doussau F, Schmidt H, Dorgans K, Valera AM, Poulain B, Isope P (2017). Frequency-dependent
680 mobilization of heterogeneous pools of synaptic vesicles shapes presynaptic plasticity. *Elife* 6.

681 51. Regehr WG (2012). Short-term presynaptic plasticity. *Cold Spring Harbor Perspect Biol* 4:a005702.

682 52. Chung CY, Seo H, Sonntag KC, Brooks A, Lin L, Isacson O (2005). Cell type-specific gene expression of
683 midbrain dopaminergic neurons reveals molecules involved in their vulnerability and protection. *Hum*
684 *Molec Genet* 14:1709-1725.

685 53. Greene JG, Dingledine R, Greenamyre JT (2005). Gene expression profiling of rat midbrain dopamine
686 neurons: implications for selective vulnerability in parkinsonism. *Neurobiol Dis* 18:19-31.

687 54. Haber SN, Ryoo H, Cox C, Lu W (1995). Subsets of midbrain dopaminergic neurons in monkeys are
688 distinguished by different levels of mRNA for the dopamine transporter: Comparison with the mRNA
689 for the D2 receptor, tyrosine hydroxylase and calbindin immunoreactivity. *J Comp Neurol* 362:400-410.

690 55. Blatow M, Caputi A, Burnashev N, Monyer H, Rozov A (2003). Ca2+ Buffer Saturation Underlies Paired
691 Pulse Facilitation in Calbindin-D28k-Containing Terminals. *Neuron* 38:79-88.

692 56. Felmy F, Neher E, Schneggenburger R (2003). Probing the Intracellular Calcium Sensitivity of
693 Transmitter Release during Synaptic Facilitation. *Neuron* 37:801-811.

694 57. Stevens CF, Williams JH (2007). Discharge of the Readily Releasable Pool With Action Potentials at
695 Hippocampal Synapses. *J Neurophys* 98:3221-3229.

696 58. Dreyer JK, Herrik KF, Berg RW, Hounsgaard JD (2010). Influence of Phasic and Tonic Dopamine Release
697 on Receptor Activation. *J Neurosci* 30:14273-14283.

698 59. Rooney KE, Wallace LJ (2015). Computational modeling of extracellular dopamine kinetics suggests low
699 probability of neurotransmitter release. *Synapse* 69:515-525.

700 60. Nanou E, Sullivan JM, Scheuer T, Catterall WA (2016). Calcium sensor regulation of the CaV2.1 Ca2+
701 channel contributes to short-term synaptic plasticity in hippocampal neurons. *Proc Natl Acad Sci USA*
702 113:1062-1067.

703 61. Sheng J, He L, Zheng H, Xue L, Luo F, Shin W, Sun T, Kuner T, Yue DT, Wu L-G (2012). Calcium-channel
704 number critically influences synaptic strength and plasticity at the active zone. *Nat Neurosci* 15:998-
705 1006.

706 62. Xu J, Wu L-G (2005). The decrease in the presynaptic calcium current is a major cause of short-term
707 depression at a calyx-type synapse. *Neuron* 46:633-645.

708 63. He Y, Zorumski CF, Mennerick S (2002). Contribution of Presynaptic Na+ Channel Inactivation to
709 Paired-Pulse Synaptic Depression in Cultured Hippocampal Neurons. *J Neurophysiol* 87:925-936.

710 64. Geiger JRP, Jonas P (2000). Dynamic Control of Presynaptic Ca2+ Inflow by Fast-Inactivating K+
711 Channels in Hippocampal Mossy Fiber Boutons. *Neuron* 28:927-939.

712 65. Ishikawa T, Nakamura Y, Saitoh N, Li W-B, Iwasaki S, Takahashi T (2003). Distinct Roles of Kv1 and Kv3
713 Potassium Channels at the Calyx of Held Presynaptic Terminal. *J Neurosci* 23:10445-10453.

714 66. Kawaguchi S-y, Sakaba T (2015). Control of inhibitory synaptic outputs by low excitability of axon
715 terminals revealed by direct recording. *Neuron* 85:1273-1288.

716 67. Ueda A, Wu C-F (2006). Distinct Frequency-Dependent Regulation of Nerve Terminal Excitability and
717 Synaptic Transmission by IA and IK Potassium Channels Revealed by Drosophila Shaker and Shab
718 Mutations. *J Neurosci* 26:6238-6248.

719 68. Bolam JP, Pissadaki EK (2012). Living on the edge with too many mouths to feed: Why dopamine
720 neurons die. *Mov Disord* 27:1478-1483.

721 69. Ofer N, Shefi O, Yaari G (2017). Branching morphology determines signal propagation dynamics in
722 neurons. *Scientific Reports* 7:8877-8877.

723 70. Brody DL, Yue DT (2000). Release-Independent Short-Term Synaptic Depression in Cultured
724 Hippocampal Neurons. *J Neurosci* 20:2480-2494.

725 71. Debanne D, Campanac E, Bialowas A, Carlier E, Alcaraz G (2011). Axon physiology. *Physiol Rev* 91:555-
726 602.

727 72. Pacelli C, Giguère N, Bourque M-J, Lévesque M, Slack Ruth S, Trudeau L-É (2015). Elevated
728 Mitochondrial Bioenergetics and Axonal Arborization Size Are Key Contributors to the Vulnerability of
729 Dopamine Neurons. *Current Biology* 25:2349-2360.

730 73. Jones SR, Gainetdinov RR, Wightman RM, Caron MG (1998). Mechanisms of amphetamine action
731 revealed in mice lacking the dopamine transporter. *Journal of Neuroscience* 18:1979-1986.

732 74. Gu H, Wall SC, Rudnick G (1994). Stable expression of biogenic amine transporters reveals differences
733 in inhibitor sensitivity, kinetics, and ion dependence. *J Biol Chem* 269:7124-7130.

734 75. McElvain JS, Schenk JO (1992). A multisubstrate mechanism of striatal dopamine uptake and its
735 inhibition by cocaine. *Biochem Pharmacol* 43:2189-2199.

736 76. Cameron KN, Solis E, Ruchala I, De Felice LJ, Eltit JM (2015). Amphetamine activates calcium channels
737 through dopamine transporter-mediated depolarization. *Cell Calcium* 58:457-466.

738 77. Smith DO (1980). Mechanisms of action potential propagation failure at sites of axon branching in the
739 crayfish. *J Physiol* 301:243-59.

740 78. Nirenberg MJ, Vaughan RA, Uhl GR, Kuhar MJ, Pickel VM (1996). The dopamine transporter is localized
741 to dendritic and axonal plasma membranes of nigrostriatal dopaminergic neurons. *J Neurosci* 16:436-
742 447.

743 79. Chen R, Daining CP, Sun H, Fraser R, Stokes SL, Leitges M, Gnegy ME (2013). Protein kinase Cbeta is a
744 modulator of the dopamine D2 autoreceptor-activated trafficking of the dopamine transporter. *J*
745 *Neurochem* 125:663-672.

746 80. McGinnis MM, Siciliano CA, Jones SR (2016). Dopamine D3 autoreceptor inhibition enhances cocaine
747 potency at the dopamine transporter. *J Neurochem* 138:821-829.

748 81. Garris PA, Wightman RM (1994). Different kinetics govern dopaminergic transmission in the amygdala,
749 prefrontal cortex, and striatum: an in vivo voltammetric study. *J Neurosci* 14:442-450.

750 82. Suaud-Chagny MF (2004). In vivo monitoring of dopamine overflow in the central nervous system by
751 amperometric techniques combined with carbon fibre electrodes. *Methods* 33:322-329.

752 83. Threlfell S, Clements MA, Khodai T, Pienaar IS, Exley R, Wess J, Cragg SJ (2010). Striatal muscarinic
753 receptors promote activity dependence of dopamine transmission via distinct receptor subtypes on
754 cholinergic interneurons in ventral versus dorsal striatum. *J Neurosci* 30:3398-3408.

755 84. Exley R, McIntosh JM, Marks MJ, Maskos U, Cragg SJ (2012). Striatal alpha5 nicotinic receptor subunit
756 regulates dopamine transmission in dorsal striatum. *J Neurosci* 32:2352-2356.

757 85. Kume-Kick J, Rice ME (1998). Dependence of dopamine calibration factors on media Ca2+ and Mg2+ at
758 carbon-fiber microelectrodes used with fast-scan cyclic voltammetry. *J Neurosci Meth* 84:55-62.

759 86. Gonon FG (1988). Nonlinear relationship between impulse flow and dopamine released by rat
760 midbrain dopaminergic neurons as studied by in vivo electrochemistry. *Neuroscience* 24:19-28.

761 87. Agus ZS, Kelepouris E, Dukes I, Morad M (1989). Cytosolic magnesium modulates calcium channel
762 activity in mammalian ventricular cells. *Am J Physiol* 256:C452-455.

763 88. Lansman JB, Hess P, Tsien RW (1986). Blockade of current through single calcium channels by Cd2+,
764 Mg2+, and Ca2+. Voltage and concentration dependence of calcium entry into the pore. *J Gen Physiol*
765 88:321-347.

766 89. van der Westhuizen ET, Valant C, Sexton PM, Christopoulos A (2015). Endogenous allosteric
767 modulators of G protein-coupled receptors. *J Pharmacol Exp Therapeut* 353:246-260.

768 90. Berggård T, Miron S, Onnerfjord P, Thulin E, Åkerfeldt KS, Enghild JJ, Akke M, Linse S (2002). Calbindin
769 D28k Exhibits Properties Characteristic of a Ca2+ Sensor. *J Biol Chem* 277:16662-16672.

770 91. Michailova A, McCulloch AD (2001). Model Study of ATP and ADP Buffering, Transport of Ca2+ and
771 Mg2+, and Regulation of Ion Pumps in Ventricular Myocyte. *Biophys J* 81:614-629.

772 92. John CE, Jones SR (2007). Voltammetric characterization of the effect of monoamine uptake inhibitors
773 and releasers on dopamine and serotonin uptake in mouse caudate-putamen and substantia nigra
774 slices. *Neuropharmacology* 52:1596-605.

775 93. Jones SR, Garris PA, Wightman RM (1995). Different effects of cocaine and nomifensine on dopamine
776 uptake in the caudate-putamen and nucleus accumbens. *J Pharmacol Exp Ther* 274:396-403.

777

778 ## Figure Legends

779 **Figure 1. Short-term plasticity at DA release sites is region-specific and only weakly release-dependent.**
780 **(A, B)** Mean profiles of $[DA]_o$ transients (± SEM) elicited by single or paired electrical pulses (*arrows*) at IPI of
781 10-200 ms in CPu (A, *n* = 4) and NAc (B, *n* = 3). Dotted traces, $[DA]_o$ attributable to the second pulse, P2, in a
782 pair (P1+P2 – P1). *Inset*, representative voltammogram for evoked DA release. **(C)** Mean P2/P1 (± SEM) vs. IPIs
783 in CPu (*filled circles*) and NAc (*open circles*). Where error bars are not visible they fall within the bounds of the
784 symbol. **(D)** P2/P1 vs peak 1p-evoked $[DA]_o$ for IPIs of 10 ms (*left*), 40 ms (*centre*) and 100 ms (*right*). Each data
785 point is 1 site in CPu (*filled circles*, *n* = 35) or NAc (*open circles*, *n* = 19). Linear fits to data show *P*-values (F-
786 test) to indicate whether the slope is significantly > 0. **(E,F)** (*Left)* Mean profiles of $[DA]_o$ transients in CPu (E, *n*
787 = 5) and NAc (F, *n* = 6) in control conditions vs L741,626 (1 µM, *green*). (*Right*) Mean P2/P1 vs IPIs in control
788 conditions and L741,626 in CPu (E) or NAc (F). Two-way ANOVA with Bonferroni's test for *post-hoc*
789 comparisons: $*P < 0.05$, $**P < 0.01$. Source data are provided as a Source Data file.

790 **Figure 2. Short-term plasticity is shaped by calcium-dependent facilitation and release-independent**
791 **depression. (A, B)** Mean profiles of $[DA]_o$ transients (± SEM) evoked by single or paired electrical pulses in 1.2
792 mM (*light grey*), 2.4 mM (*dark grey*) and 3.6 mM (*black*) $[Ca^{2+}]_o$ in CPu (A, *n* = 3) and NAc (B, *n* = 3). **(C)** Mean
793 1p evoked $[DA]_o$ (± SEM, normalised to 2.4 mM $[Ca^{2+}]_o$) vs $[Ca^{2+}]_o$ in CPu (*filled*) and NAc (*open circles*). **(D, E)**
794 Mean P2/P1 (± SEM) vs. IPI in 1.2 mM (*light grey*), 2.4 mM (*dark grey*) and 3.6 mM (*black*) $[Ca^{2+}]_o$ in CPu (D,
795 *filled*) and NAc (D, *open circles*). **(F)** Mean P2/P1 (± SEM) vs mean peak 1p $[DA]_o$ (± SEM) at 10 ms IPI in 1.2 mM
796 (*light grey*), 2.4 mM (*dark grey*) and 3.6 mM (*black*) $[Ca^{2+}]_o$ in CPu (*filled*) and NAc (*open circles*). **(G)** Mean
797 profiles of $[DA]_o$ transients (± SEM) elicited by single or paired light pulses at 40 ms IPI (473 nm, 2 ms) in 1.0
798 mM (*light grey*), 2.0 mM (*dark grey*) and 3.0 mM (*black*) $[Ca^{2+}]_o$ in CPu (*left*, *n* = 3) and NAc (*right*, *n* = 3). *Inset*,
799 representative voltammogram for optogenetically voked DA release. **(H)** Mean peak 1p $[DA]_o$ (± SEM,
800 normalised to 2.4 mM $[Ca^{2+}]_o$) vs $[Ca^{2+}]_o$ (log scale) evoked by light stimulation in CPu (*filled*) and NAc (*open*
801 *circles*). Second-order polynomial curve fit; F-test of relative sum of squares shows curve fits are different. **(I)**
802 Mean P2/P1 (± SEM) at 40 ms IPI vs mean peak 1p $[DA]_o$ (± SEM) evoked by optical stimulation in CPu (*filled*)

803 and NAc (*open circles*). Two-way ANOVA with Bonferroni's test for *post-hoc* comparisons except where stated
804 otherwise: *P < 0.05, **P < 0.01, ***P < 0.001. Source data are provided as a Source Data file.

805 **Figure 3. A release-insensitive mechanism of short-term depression is controlled by [K^+]-dependent gating.**
806 **(A, B)** Mean profiles of $[DA]_o$ (± SEM) elicited by single or paired electrical pulses in 1.25 mM (*light grey*), 5 mM
807 (*dark grey*) and 7.5 mM $[K^+]_o$ (*black*) in CPu (A, n = 3) and NAc (B, n = 3). **(C, D)** Mean P2/P1 (± SEM) vs IPIs in
808 1.25 mM (*light grey*), 5 mM (*dark grey*) and 7.5 mM $[K^+]_o$ (*black*) in CPu (C) and NAc (D). **(E)** Mean P2/P1 (±
809 SEM) vs. mean peak 1p $[DA]_o$ (± SEM) in 1.25 mM (*light grey*), 5 mM (*dark grey*) and 7.5 mM (*black*) $[K^+]_o$ in
810 CPu (*filled*) and NAc (*open circles*) at 10 ms IPI (*left*) and 100 ms IPI (*right*). Two-way ANOVA with Bonferroni's
811 test for *post-hoc* comparisons; *P < 0.05, ***P < 0.001. Source data are provided as a Source Data file.

812 **Figure 4. K^+-dependent gating of short-term depression requires axonal Kv channels. (A, E)** Mean profiles of
813 $[DA]_o$ transients (± SEM) in CPu elicited by single or paired electrical pulses in control conditions (*black*) or with
814 100 µM 4-AP (*grey*) in CPu (A, n = 4) and NAc (E, n = 3). Data are normalised to peak 1p-evoked $[DA]_o$ (P1) in
815 control conditions (*vertical scale bars*). **(B, F)** Mean 1p $[DA]_o$ (± SEM) in CPu in 1 mM and 5 mM $[K^+]_o$ in control
816 conditions (*black/grey*) or 4-AP (*reds*) in CPu (B) or in NAc (F). **(C, G)** Mean P2/P1 (± SEM) in CPu vs IPI in 5 mM
817 (*black*) and 1 mM (*grey*) $[K^+]_o$ in control conditions (*left*) and 4-AP (*right*) in CPu (C) and in NAc (G). **(D, H)** Mean
818 P2/P1 (± SEM) in CPu at 25 ms IPI in 1 mM and 5 mM $[K^+]_o$ in control conditions or 4-AP in CPu (D) and in NAc
819 (H). (D), asterisks indicate interaction between $[K^+]_o$ and 4-AP. Two-way ANOVA with Bonferroni's test for *post-*
820 *hoc* comparisons; *P < 0.05, **P < 0.01. Source data are provided as a Source Data file.

821 **Figure 5. K^+-dependent gating does not alter release-dependence of short-term plasticity. (A,B,E,F)** Mean
822 profiles of $[DA]_o$ transients (± SEM) elicited by single or paired pulses in 1.2 mM $[Ca^{2+}]$ (*light grey*), 2.4 mM
823 $[Ca^{2+}]_o$ (*dark grey*) and 3.6 mM $[Ca^{2+}]_o$ (*black*) in either 5 mM $[K^+]_o$ (*A,E*) or 1 mM $[K^+]_o$ (*B,F*) in CPu (A,B, n = 11)
824 and in NAc (E,F, n = 7). **(C, G)** Mean peak 1p $[DA]_o$ (± SEM, normalised to 2.4 mM $[Ca^{2+}]_o$) in 5 mM $[K^+]_o$ (*black*)
825 and 1 mM $[K^+]_o$ (*grey*) in CPu (C) and in NAc (G). **(D, H)** Mean P2/P1 (± SEM) at 10 ms IPI (*left*) and 100 ms IPI

826 (*right*) in 5 mM $[K^+]_o$ (*black*) and 1 mM $[K^+]_o$ (*grey*) in CPu (D) and in NAc (H). Two-way ANOVA with Bonferroni's
827 test for *post-hoc* comparisons. Source data are provided as a Source Data file.

828 **Figure 6. The dopamine transporter regulates short-term plasticity of dopamine release. (A, G)** Mean profiles
829 of $[DA]_o$ transients (± SEM) elicited by single or paired electrical pulses in control conditions (*black*) or with 5
830 µM cocaine (*blue*) in CPu (A, *n* = 4) or NAc (G, *n* = 4). **(B, H)** Mean P2/P1 (± SEM) against IPI in control conditions
831 (*black*) and with cocaine (*blue*) in CPu (B) or NAc (H). **(C, I)** Mean profiles of $[DA]_o$ transients (± SEM) elicited by
832 single or paired electrical pulses in control conditions (*black*) or with 5 µM methylphenidate (*MPH*, *grey*) in
833 CPu (C, *n* = 5) or NAc (G, *n* = 3). **(D, J)** Mean P2/P1 (± SEM) vs IPI in control conditions (*black*) and with MPH
834 (*green*) in CPu (D) or NAc (J). **(E)** Mean profiles of $[DA]_o$ transients (± SEM) elicited by single or paired electrical
835 pulses in control conditions (*black*) or with 10 µM nomifensine (*red*) in CPu (*n* = 3). **(F)** Mean P2/P1 (± SEM) vs
836 IPI in control conditions (*black*) and with nomifensine (*red*) in CPu. Two-way ANOVA with Bonferroni's test for
837 *post-hoc* comparisons; $*P < 0.05$, $**P < 0.01$, $***P < 0.001$. Source data are provided as a Source Data file.

838 **Figure 7. The DAT limits release-dependence of short-term plasticity in CPu. (A)** Mean profiles of $[DA]_o$
839 transients (± SEM, vertical scale normalised to 1p in 2.4 mM $[Ca^{2+}]_o$) (*n* = 4) elicited by single or paired electrical
840 pulses in 2.4 mM (*upper*) and 1.2 mM $[Ca^{2+}]_o$ (*lower*) in control conditions (*black*) or 5 µM cocaine (*blue*). **(B,**
841 **C)** Mean P2/P1 (± SEM) vs. IPI in 1.2 mM (*light*) and 2.4 mM $[Ca^{2+}]_o$ (*dark*) in control conditions (B) or cocaine
842 (C). **(D)** Mean P2/P1 (± SEM) in 1.2 mM and 2.4 mM $[Ca^{2+}]_o$ in control conditions (*black-grey*) or cocaine (*blue*)
843 at 25 ms IPI (*left*) or 40 ms IPI (*right*). Two-way ANOVA with Bonferroni's test for *post-hoc* comparisons; $*P <$
844 0.05, $**P < 0.01$, $***P < 0.001$. Source data are provided as a Source Data file.
845

846 **Figure 8. The DAT and $[K^+]_o$ gate short-term plasticity through overlapping mechanisms. (A,E)** Mean profiles
847 of $[DA]_o$ transients (± SEM) elicited by single or paired electrical pulses in control conditions or cocaine in 5
848 mM $[K^+]_o$ (*upper*) and 1 mM $[K^+]_o$ (*lower*) in CPu (A, *n* = 4) and in NAc (E, *n* = 3). **(B, F)** Mean P2/P1 (± SEM) vs.
849 IPI in 5 mM $[K^+]_o$ (*black*) and 1 mM $[K^+]_o$ (*grey*) in control conditions (*left*) or cocaine (*right*) in CPu (B) and in

850 NAc (F). **(C, G)** Mean 1p $[DA]_o$ (± SEM) in control conditions (*black-grey*) or cocaine (*blue*) in CPu (C) and in NAc
851 (G). **(D, H)** Mean P2/P1 (± SEM) in CPu at 25 ms IPI in 1 mM and 5 mM $[K^+]_o$ in control conditions or with cocaine
852 in CPu (D) and in NAc (H). Two-way ANOVA with Bonferroni's test for *post-hoc* comparisons; $*P < 0.05$, $**P <$
853 0.01. Source data are provided as a Source Data file.
854
855 **Figure 9. The DAT and $[K^+]_o$ gate intracellular Ca^{2+} dynamics during paired-pulse stimulations.**
856 **(A)** Images of VTA and SNc from DAT-Cre:Ai95D mice showing GCaMP6f eGFP expression (*green*) in TH-positive
857 neurons (*red*). **(B,D)** Examples of Ca^{2+}-imaging responses (changes to GCaMP6f fluorescence, ΔF/F) (mean ±
858 SEM from duplicate) in DA axon population imaged in CPu in response to single or paired electrical pulses at
859 IPI of 10 and 40 ms in (B) 5mM $[K^+]_o$ (*grey*) or 7.5 mM $[K^+]_o$ (*black*), or (D) in control conditions (*black*) or the
860 presence of cocaine (5 µM) (*blue*). Data are rescaled to 1p in each condition to control for photobleaching.
861 **(C,E)** Mean peak values (± SEM) for GCaMP6f ΔF/F evoked by 2 pulses vs. IPI. Data are normalised to value for
862 1 pulse (N = 5 animals). Two-way ANOVA with Fishers LSD test for *post-hoc* comparisons: $*P < 0.05$, $**P < 0.01$,
863 $***P < 0.001$. DHβE (1 µM) is present throughout. Source data are provided as a Source Data file.

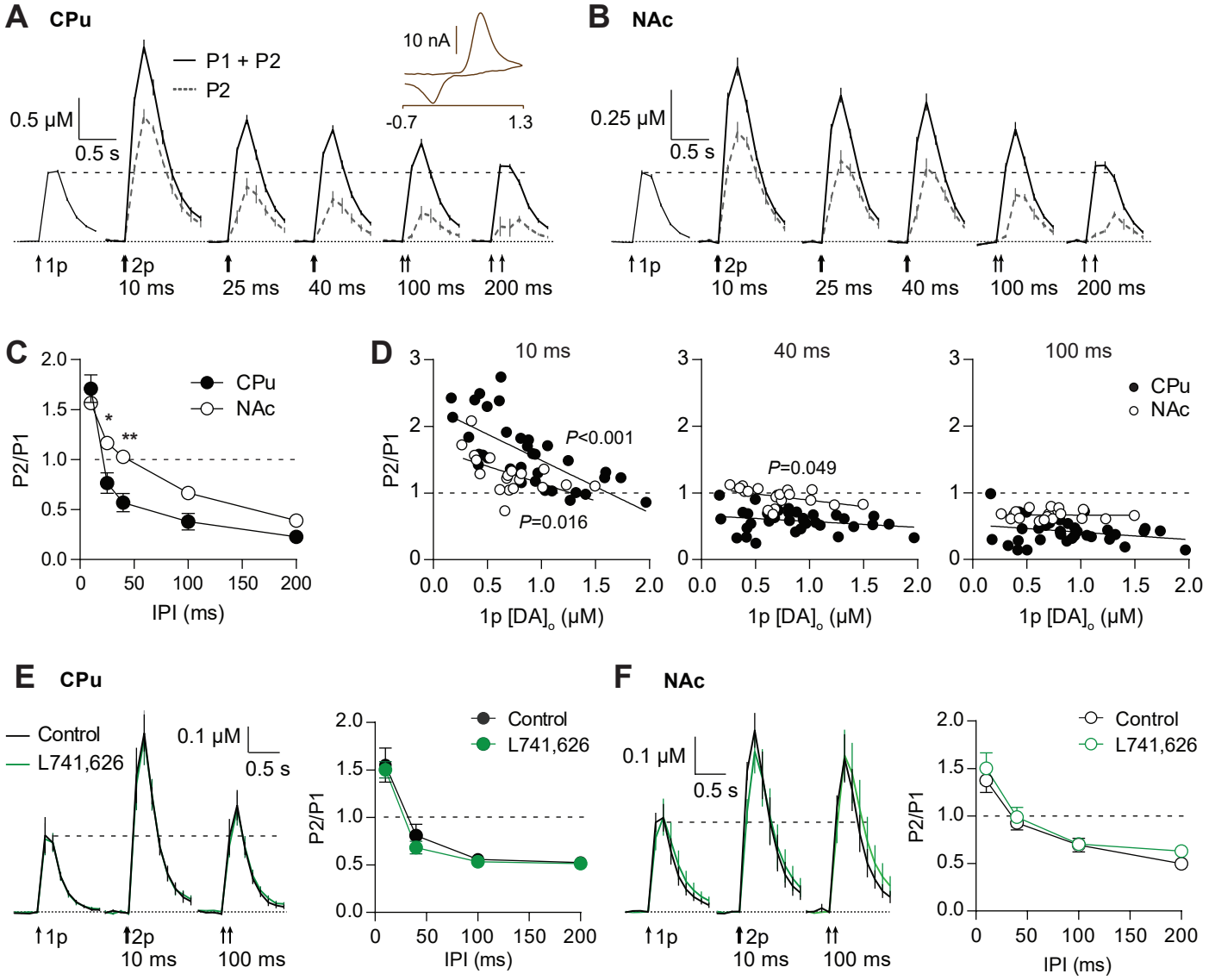

Figure 1
Condon et al

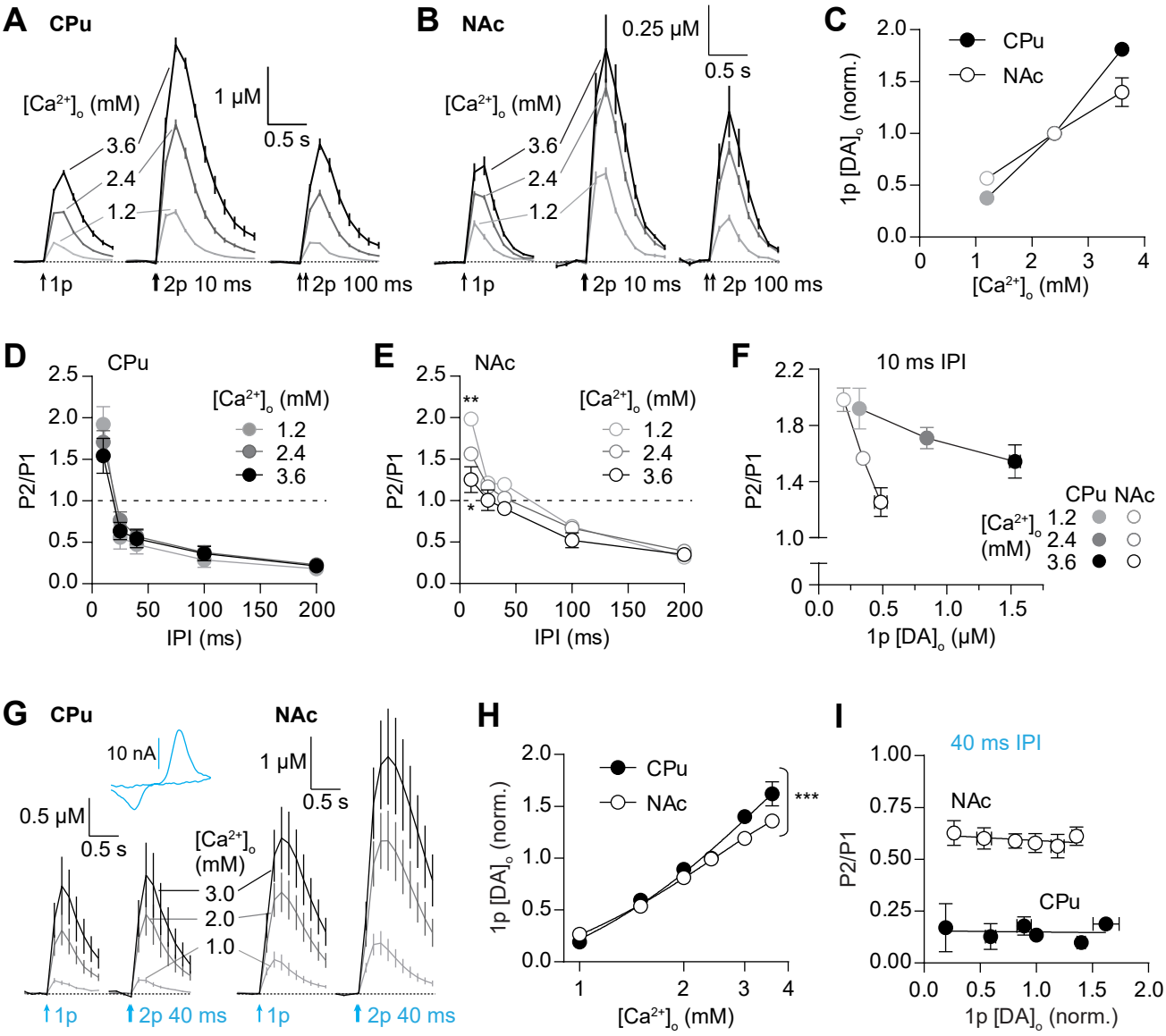

Figure 2
Condon et al

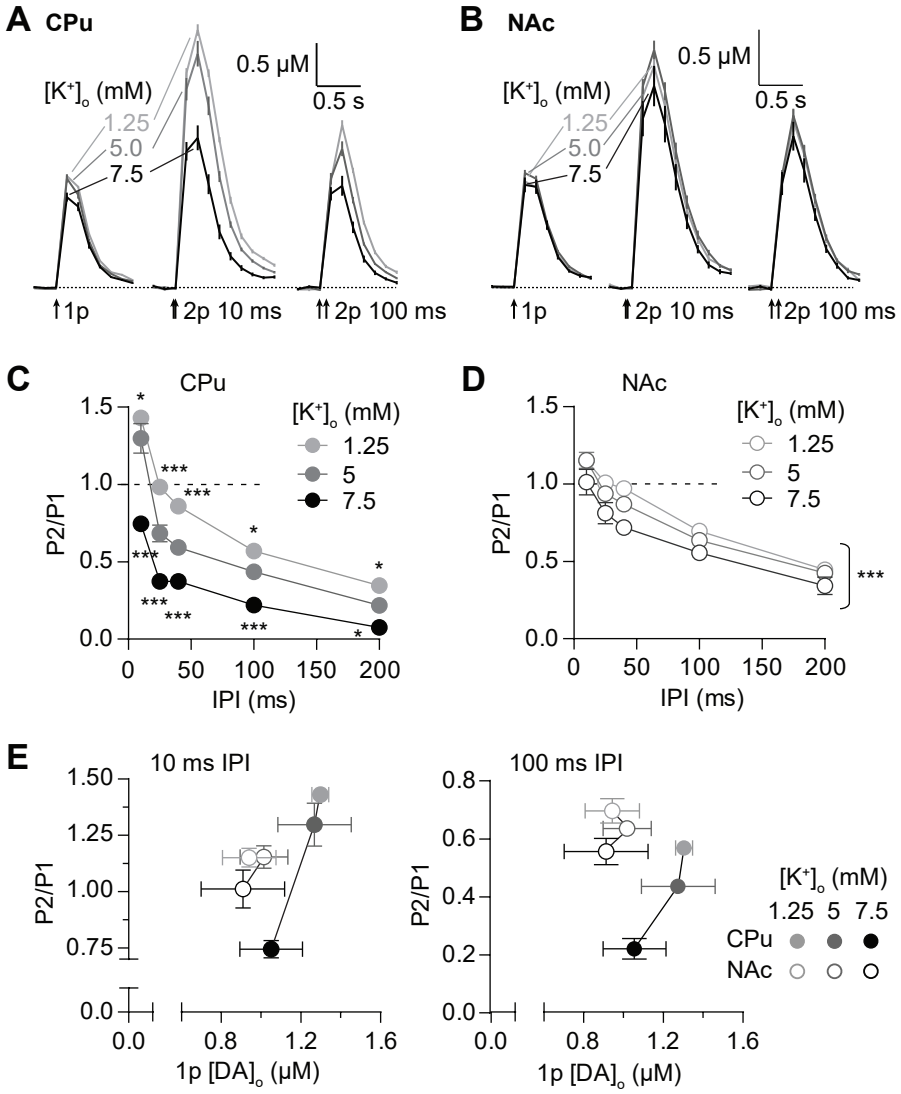

Figure 3
Condon et al

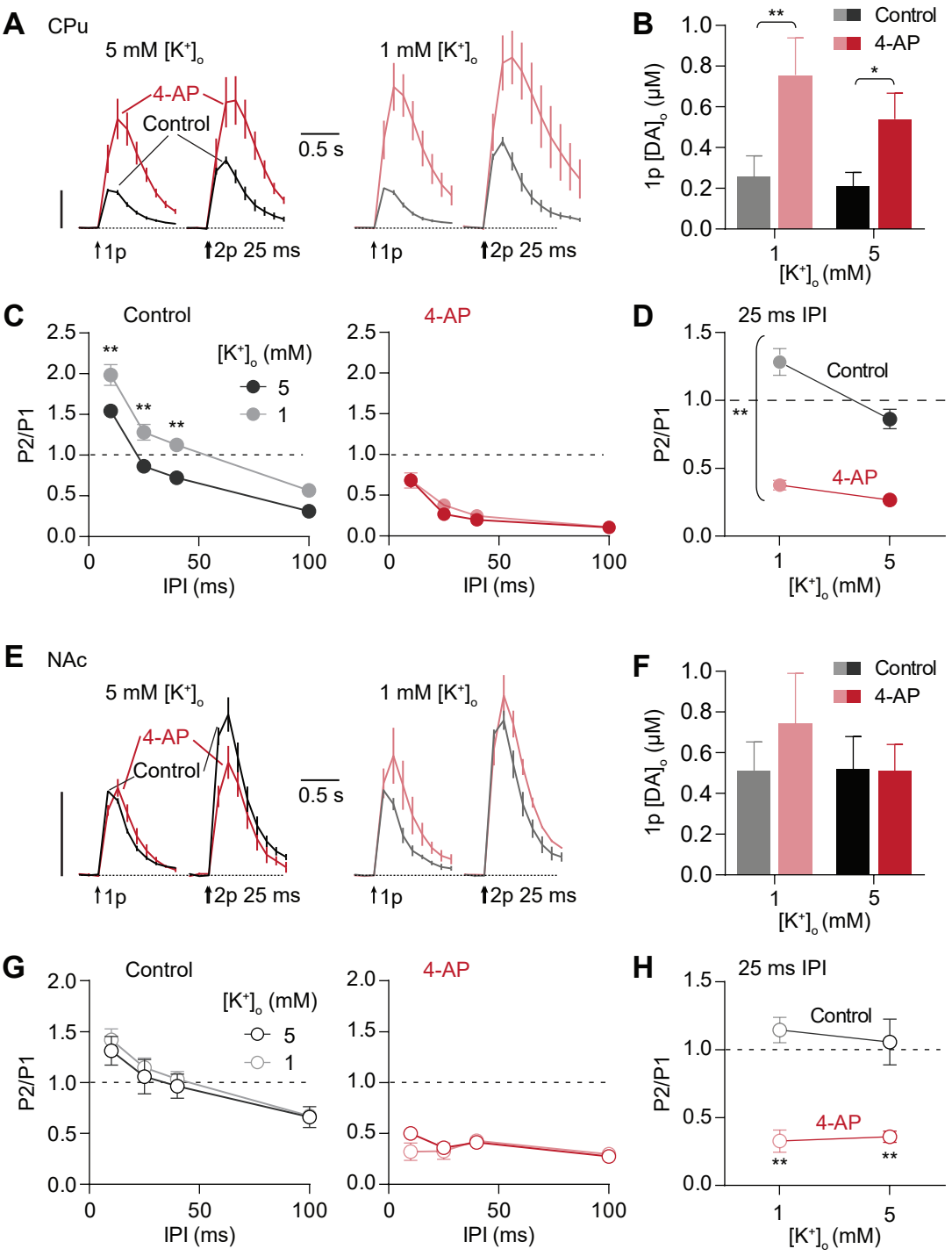

Figure 4
Condon et al

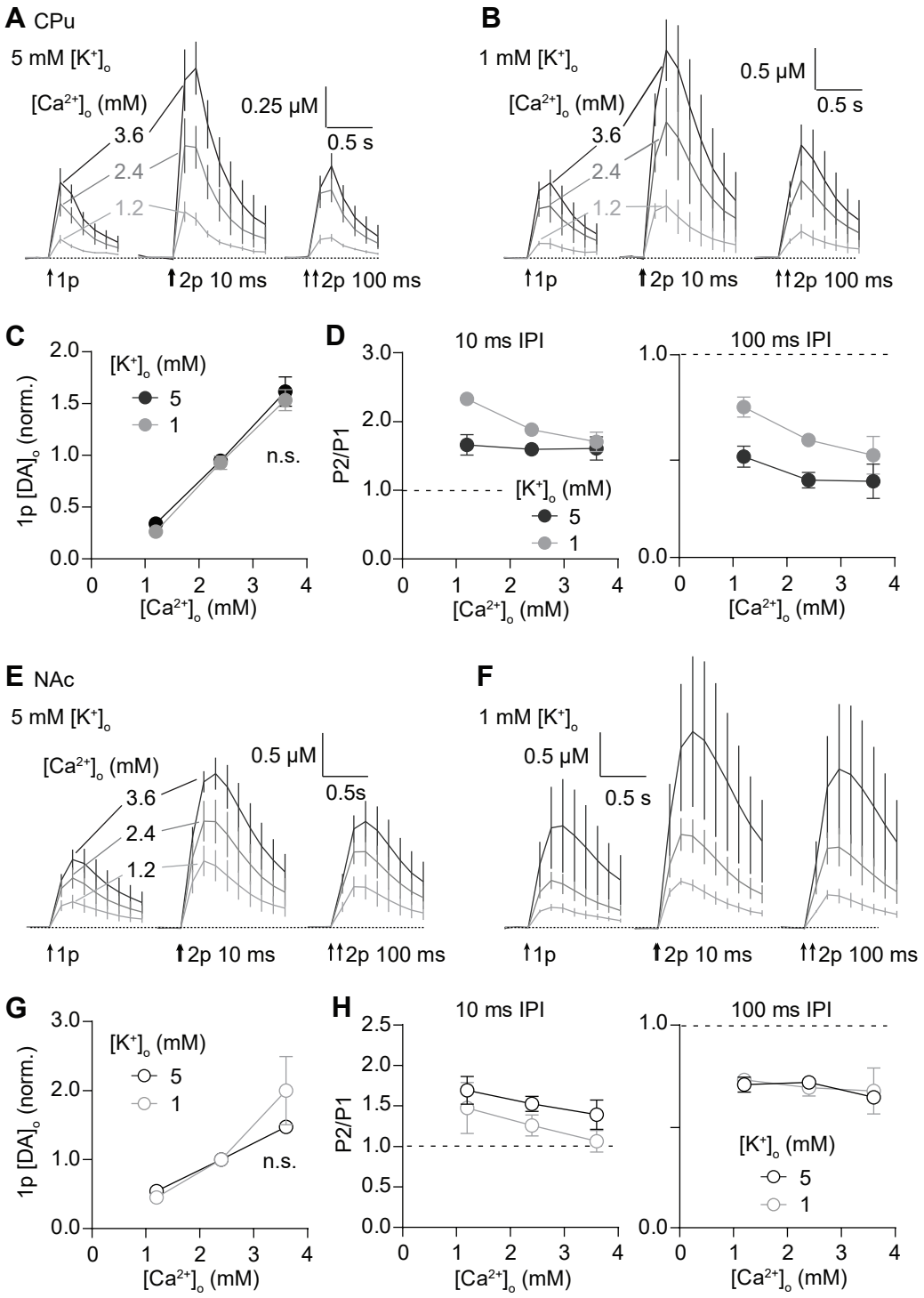

Figure 5
Condon et al

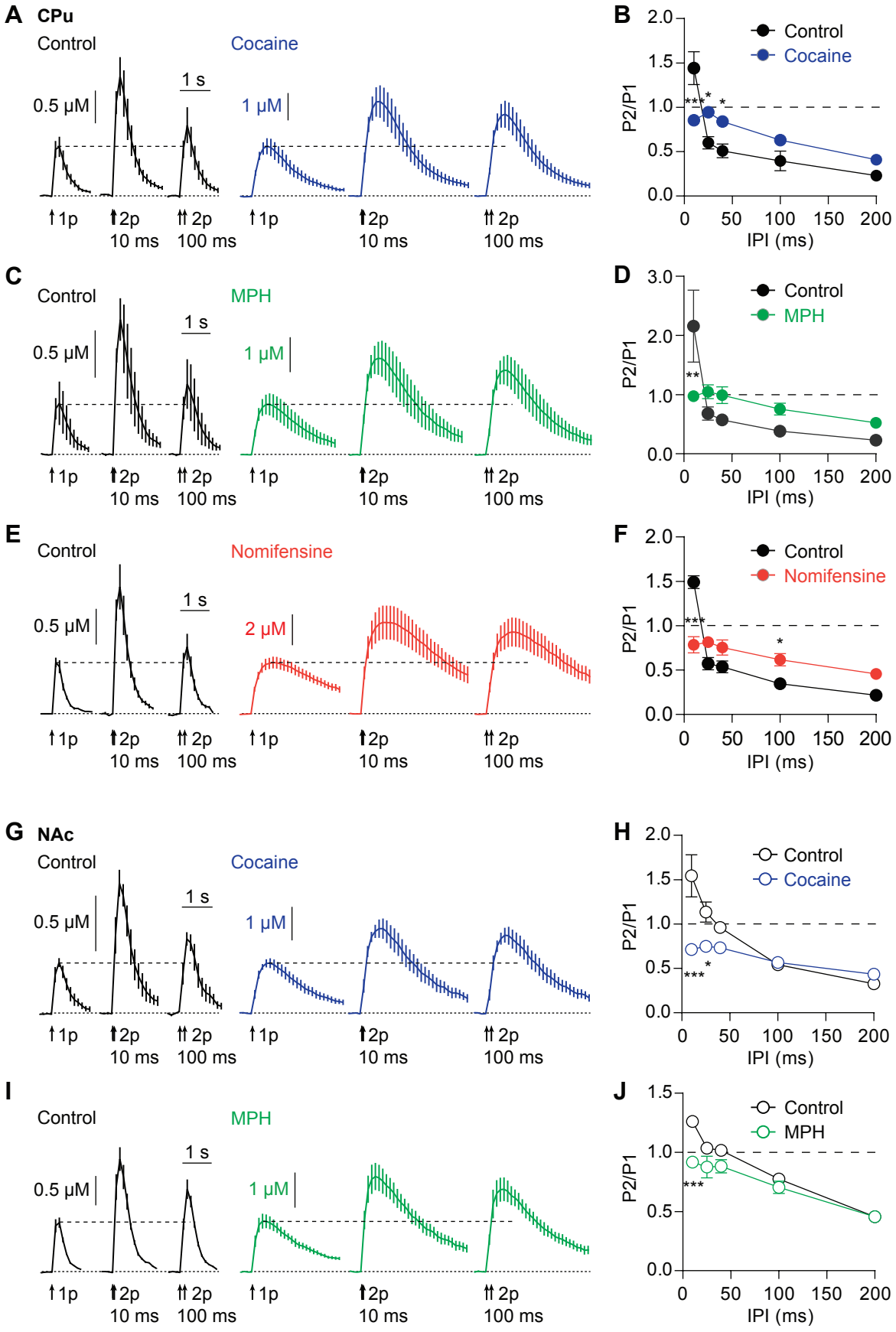

Figure 6
Condon et al

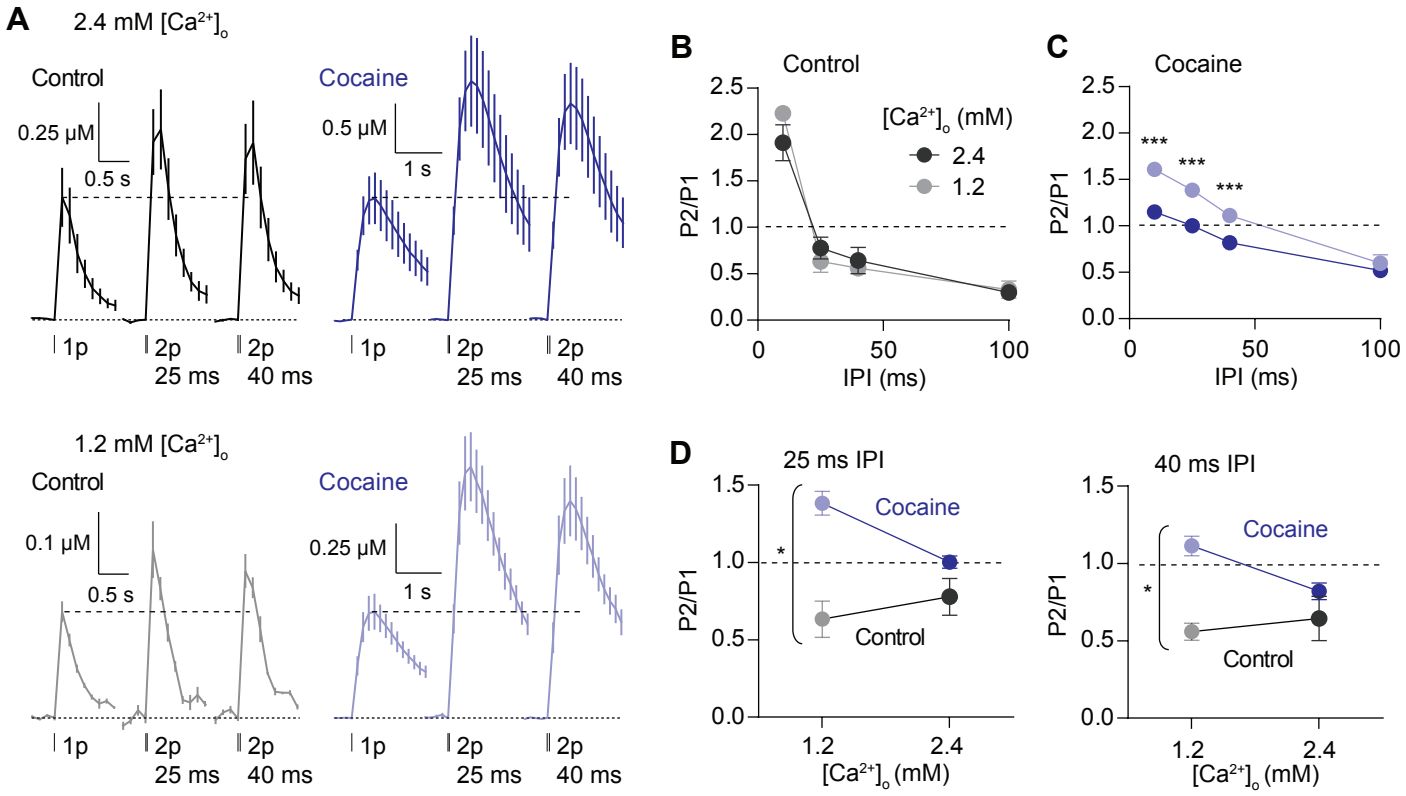

Figure 7
Condon et al

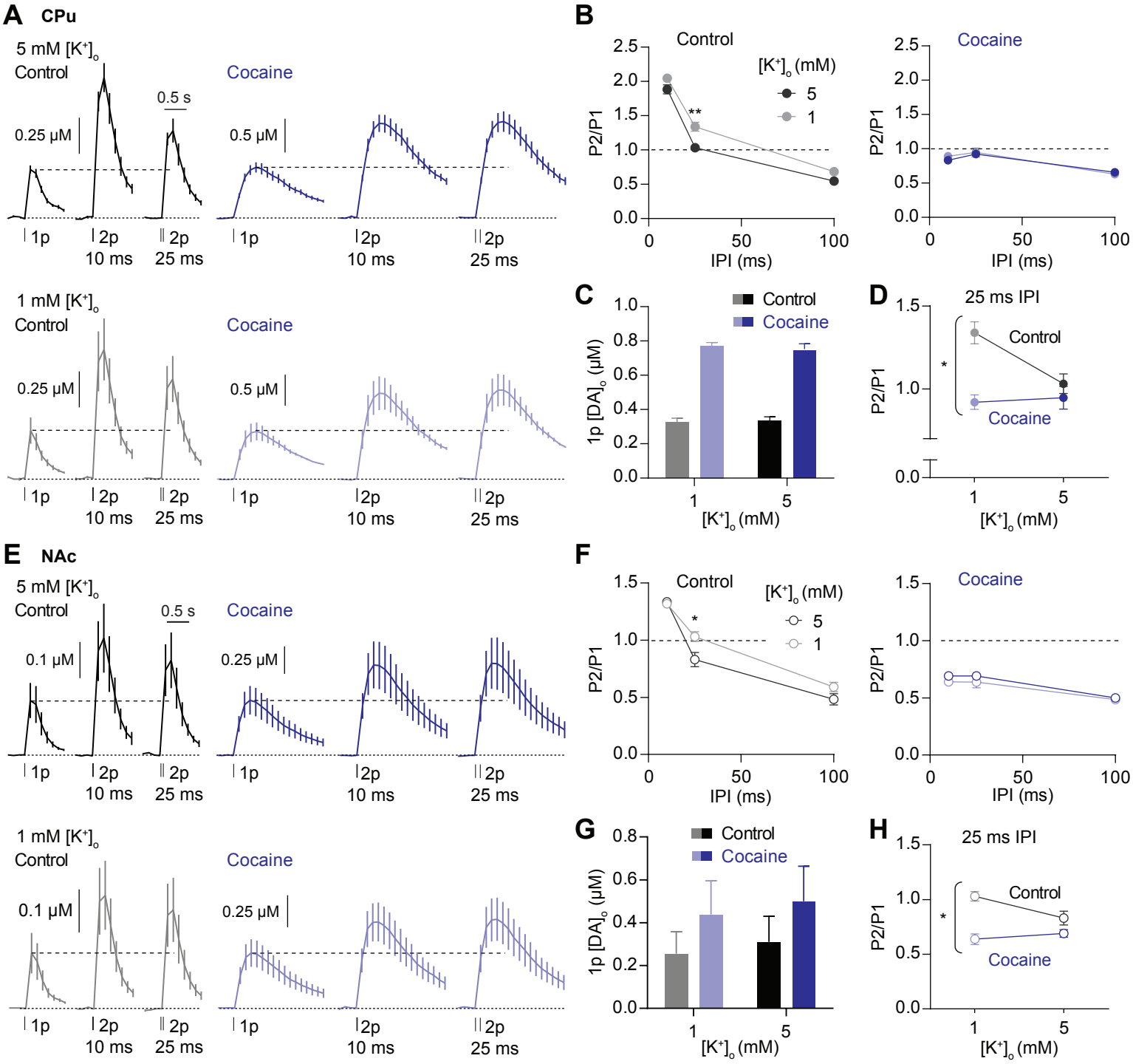

Figure 8
Condon et al

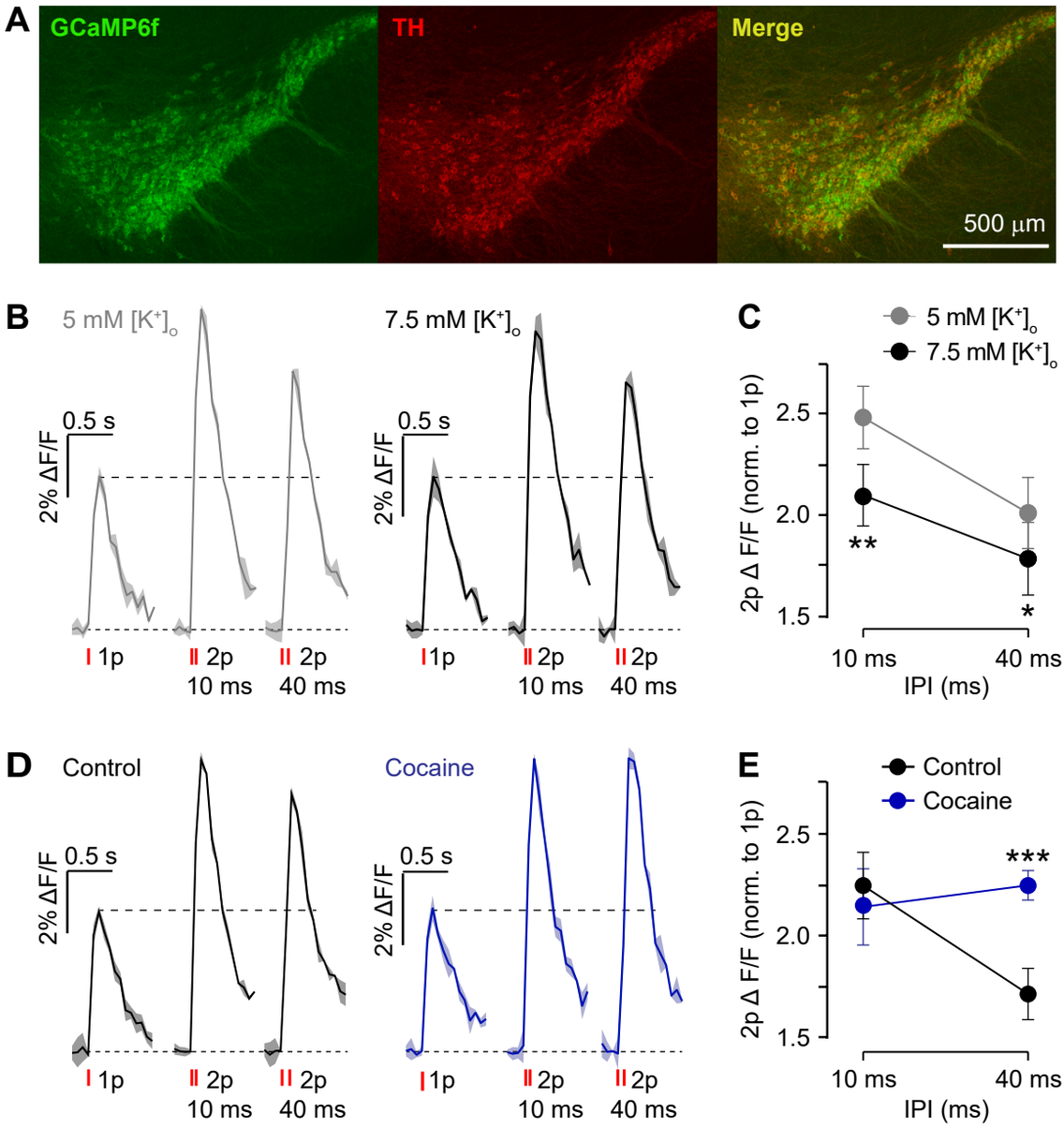

Figure 9
Condon et al